Can a Growth Hormone-Derived Peptide (AOD9604) Prevent Bone Loss and Fragility in a Rat Model of Osteoporosis?

by

Elisabeth Jane Rowe

A thesis submitted in conformity with the requirements
for the degree of Master of Applied Science
Graduate Department of Materials Science and Engineering
University of Toronto

Your file Votre référence
ISBN: 978-0-494-27369-2
Our file Notre référence
ISBN: 978-0-494-27369-2

Abstract

Can a Growth Hormone-Derived Peptide (AOD9604) Prevent Bone Loss and Fragility in a Rat Model of Osteoporosis?

Elisabeth Jane Rowe

Master of Applied Science

Graduate Department of Materials Science and Engineering

University of Toronto

2007

A synthetic human Growth Hormone (hGH) 16AA C–terminus peptide, AOD9604 (AOD, Tyr-hGH$_{171-191}$), has been shown to modulate fat metabolism and is currently being developed as a novel weight-loss drug. However, intact hGH affects the skeleton as well as lipids. This current study identified similar skeletal effects with the hGH peptide and assessed the ability of AOD to prevent OVX-induced bone loss and fragility. Two different dosages (0.25mg/kg/day, AOD–0.25 and 0.5mg/kg/day, AOD–0.5) of orally administered drug were administered over a 12–wk period in the ovariectomized (OVX) rat. Bone mass, mechanics, material and structural parameters were assessed. Overall, we evidenced that both doses of AOD prevented OVX–induced fragility and bone loss in cortical bone. In trabecular bone, AOD–0.25 prevented OVX–induced fragility and attenuated bone formation and bone loss and these trabecular improvements were not evident with AOD–0.5.

Acknowledgements

The past two years have been a roller coaster of challenges and successes and I have several people to thank for helping to celebrate the ups and pull me through the downs.

First and foremost, I would like to thank my supervisor, Dr. Marc Grynpas, for always pushing me one step further; forcing me to question and for the subtle reminders of Biology's complexities and where the field swerves from Engineering. I would also like to acknowledge my committee members, Dr. Rita Kandel and Dr. Robert Pilliar, for their helpful suggestions and careful edits.

This work would not have been completed without technical assistance. At the front end, Dr. Richard Renlund had a large part in the study design and the care and treatment of the animals. Dr. Mircea Dumitriu, the self-acclaimed "strut wizard" worked miracles in transforming my images into useful data. These images would not have been possible without the assistance of Doug Holmyard, who always caught me at the low parts of the roller coaster with a new analysis technique.

I would also like to acknowledge the members of the Grynpas Lab. Their endless support, humour and love of Japanese food along with their proven brilliance have made this ride enjoyable. I would especially like to thank my lab manager, Richard Cheung, for being so efficient and attentive and Dr. Sidney Omelon for exercising her genuine love of learning and helping me to format this thesis. On that note, I should also acknowledge Robert Pitt, who developed the Latex template for UofT theses.

Finally, I would like to thank Bill for his mechanical expertise and unconditional support.

Contents

List of Tables

List of Figures

Chapter 1

Introduction

1.1 Motivation

A startling 59% of adult Canadians are overweight or obese (CCHS Data, 2004). Furthermore, obesity increases the risk of chronic preventable diseases such as heart disease, diabetes and some cancers (MacDonald et al., 1997). Therefore, there is a need for an effective and tolerable anti-obesity drug. To supply this demand, a synthetic human Growth Hormone (hGH) 16AA C-terminus peptide, (AOD9604, Tyr-hGH$_{177-191}$), which has been shown to modulate fat metabolism, is currently being developed as a novel weight-loss drug. However, intact hGH has well known skeletal effects as it is best known for regulating postnatal skeletal growth (Canalis, 1995). Therefore, we need to understand if any of these skeletal effects are conserved in the peptide.

1.2 Bone Background

To develop an understanding of bone pathology and responses to treatment we must first consider bone structure, composition, cells and bone remodeling. While it is convenient to separate these aspects, they are in fact interrelated such that a change in one induces change in another, thereby altering overall bone behaviour.

1.2.1 Bone Structure

Bone is a three dimensional composite material with several levels of organization in order to best satisfy needs of mobility, support and chemical balance.

At the highest level of organization, we can distinguish long bones such as the femur and the tibia in the leg to other types of bone such as the cuboid vertebrae in the spine. Long bones support the body from bending, torsion and compression forces while the cuboid bones support from complex stress states and play a significant role in chemical balance.

Bones themselves are each composed of two different types of bone: cortical and trabecular. Cortical bone is relatively dense as it has four times the mass of trabecular bone. Cortical bone comprises the diaphysis of long bones providing the required strength but also surrounds cuboid bones for protection. Contrarily, trabecular bone is porous since it is composed of internal spicules (trabeculae) which are oriented along lines of stress. Trabecular bone can be found at the metaphysis/epiphysis of long bones as well as the interior of cuboid bones.

Both cortical and trabecular bone have different microstructures. Human cortical bone is comprised of osteons, which are vascular channels surrounded by concentric layers of lamellar bone. These osteons are oriented along the long axis of the bone. While this is true of human bone, rat bone has a rotated plywood structure of primary lamellar bone (Weiner et al., 1997). Trabecular bone in both humans and rats is composed of layered lamellar bone.

Within lamellae, there is an organization of inorganic and organic phases, which will be further discussed in terms of bone composition.

1.2.2 Bone Composition

Bone is approximately 60–70% mineral, 5–8% water and the remainder is an organic phase. This organic phase is composed of approximately 90% type I collagen while non-collageneous matrix proteins, minor collagen types, lipids and macromolecules constitute the remainder (Kaplan et al., 1994).

The mineral is a poorly crystalline calcium phosphate called hydroxyapatite (HA), which has the following stoichiometric formula: $Ca_{10}(PO_4)_6(OH)_2$ (Kaplan et al., 1994). Substitutions are common, which can change the biological properties.

Collagen has a highly organized structure. It consists of three polypeptide chains with 1000 amino acids in each, which form a triple helix. This creates a rigid and linear molecule that is 300 nm in length. Collagen molecules are aligned in parallel in a staggered formation, which leaves gaps, hole zones and pores. This formation makes up a collagen fibril. Several fibrils then gather together into bundles to form a collagen fiber (Kaplan et al., 1994).

There is a strong interface between collagen and the mineral which occurs through a process called mineralization. There are three steps in this process. Firstly, crystals nucleate, which is thought to occur in hole zones between collagen molecules. Secondly, these crystals grow and finally more crystals nucleate on interfaces created by the original crystals. In this manner, as bone regions age they become more mineralized (Burnell et al, 1980). However, within each bone there are varying degrees of mineralization due to bone modeling and remodeling, which are carried out by specialized bone cells.

1.2.3 Bone Cells

Bone has three specialized cell types: the osteoblast, the osteocyte and the osteoclast.

Osteoblasts are bone forming cells. They line bone surfaces and produce matrix elements including typeI collagen, osteocalcin, osteopontin, proteoglycans and regulating

factors. Osteoblasts contain a single nucleus and organelles for this protein manufacture and secretion (Kaplan et al., 1994).

Osteocytes are osteoblasts that have been trapped within the mineralized matrix. Osteocytes contain a large nucleus but fewer organelles than the osteoblast. Based on their position and cell composition, osteocytes are thought to provide communication with subsurface bone (Kaplan et al., 1994).

Osteoclasts are bone resorbing cells. They are large (20-100 μm diameter), multi-nucleated cells derived from hematopoetic precursors. Osteoclasts bind to the bone surface and resorb bone underneath the attachment area. This resorption is achieved through production of hydrogen ions, which lower the pH and consequently increase the solubility of HA crystals. The organic matrix is then degraded via acidic proteolytic digestion (Kaplan et al., 1994).

1.2.4 Bone Remodeling

One of the most unique properties of bone is its ability to remodel itself. This is a biological activity involving the coupling of the bone resorbing cells, the osteoclasts, and the bone forming cells, the osteoblasts.

Ideally, the processes of the bone cells are coupled to provide a healthy tissue. However, the resorption and formation processes are not always in balance. During the bone modeling of skeletal growth, formation dominates; however, around 30 years of age the balance shifts such that resorption exceeds formation and there is a net bone loss. This imbalance results in the gradual decrease in bone mass of an individual over a lifetime (Kaplan et al., 1994).

Remodeling is a surface phenomenon due to the osteoblast cell lining on bone surfaces. Cortical and trabecular bone provide significantly different surface areas and therefore the cell numbers and consequently remodeling rates in the two bone types differ. In cortical bone, remodeling occurs on the periosteal, endosteal and haversian canal surfaces.

In trabecular bone, remodeling occurs on the trabeculae. Therefore, trabecular bone can reach 5-10 times the cortical remodeling rates (Eriksen et al., 1994). As a result, the effects of diseases and treatments that effect remodeling are more pronounced in trabecular bone.

The rate of remodeling is known to be affected by several factors but most notably hormones. Sex hormones including testosterone and estrogen are responsible for both growth after puberty and deterioration in later years.

1.3 Postmenopausal Osteoporosis

Osteoporosis is a metabolic bone disease that is characterized by decreased bone mass and connectivity as well as changes in material properties. This leads to increased bone fragility and ultimately an increased fracture risk (Wasnich, 1996). There are two types of osteoporosis: age-related and post-menopausal. While age-related is a result of a gradual decline in bone formation with aging, post-menopausal is a result of increased remodeling.

At the menopause, the cessation of estrogen causes an increase in both resorption and formation; however, the increase in resorption is greater than the increase in formation, which leads to a net bone loss (Eastell et al., 1998). Effects are most pronounced in trabecular bone due to the larger available surface area although some cortical bone loss also occurs.

1.3.1 The Aged Rat Model of Postmenopausal Osteoporosis

The rat is an established and preferred model for preclinical assessment of the pathology of postmenopausal osteoporosis and possible treatments since it is economical, easily controlled, changes can be observed quickly and it is similar to humans. The aged rat is preferred to the young rat since the skeleton at 9 months has stopped growing, which is

comparable to the mature human skeleton (Kalu et al., 1989).

Ovariectomy (OVX) in the rat results in estrogen deficiency and significant bone loss, which is similar to postmenopausal women (Kalu, 1991; Wronski and Yen, 1991). Furthermore, the trabecular bone loss is greater than that of cortical bone (Kalu, 1991; Wronski and Yen, 1991; Baldock et al. 1999). Assessment of mechanical properties shows that OVX causes a decrease in trabecular (vertebral and femoral neck) strength and stiffness (Bagi et al., 1997; Mosekilde et al., 1998; Turner et al., 1994). Assessment of bone turnover shows an increase in new bone (osteoid) volume and assessment of structure reveals lower bone volume and decreased trabecular connectivity (Baldock et al., 1999).

1.4 Bone Quality

In clinic, we are ultimately concerned with a patient's susceptibility to fracture. This has traditionally been assessed by measurement of bone mass or bone mineral density. However, this quantitative parameter does not provide an adequate assessment as it ignores bone's complex material and structural properties. In 1993, Heaney grouped these properties into the concept of bone quality and introduced this as an additional predictor of fracture susceptibility (Heaney, 1993). Therefore, fracture risk, which can be equated to the mechanical properties of bone, is dependent on material properties such as mineralization and structural properties such as structure and the connectivity of trabeculae. Furthermore, both the material and structural properties are influenced by bone remodeling.

1.4.1 Assessment of Bone Mineral Density: Dual Energy X–Ray Absorptiometry

Bone mineral density (BMD) as measured by Dual Energy X–Ray Absorptiometry (DXA) is an areal density rather than a volumetric one. Nevertheless, it is a quantitative technique that indicates the amount and density of bone and since it is non-invasive it is a useful and common clinical measure. A decrease in BMD has been shown to correlate with fracture risk (Council of the National Osteoporosis Foundation, 1996). BMD has also been shown to correlate to bone strength, although not as a sole predictor (Hansson et al., 1980; Leichter et al., 1982).

The technique involves exposing a sample to both low and high energy x-rays. The low energy x-rays pass through soft tissue only while the high energy x–rays pass through both the soft tissue and the hard bone tissue. Therefore, the difference between the x-rays reaching the detector reflects the energy absorbed by the bone and similarly the amount of bone. The resulting parameter is referred to as bone mineral content (BMC) and when divided by the two dimensional projected area of the bone it becomes bone mineral density (BMD). The precision and accuracy of this technique has been confirmed (Pouilles et al., 1991; Wahner, 1989). DXA has also been validated for BMD in the rat (Griffin et al., 1993; Nagy et al., 2001; Gala et al., 1998; Sato et al., 1994). Furthermore, DXA tests on excised lumbar vertebrae and femur have also been shown to provide trabecular and cortical densities respectively (Nagy et al., 2001; Sato et al., 1994).

1.4.2 Assessment of Mechanical Properties

Since mechanical properties are directly related to fracture risk, they are a much stronger predictor of mechanical integrity and propensity to failure than BMD measurements. However, mechanical testing is invasive and therefore can only be performed in animal models. Tests must be designed to best reproduce either the normal or the pathological

conditions in question. This is dependent on several conditions, which include but are not limited to: rate and direction of testing, method of measurement, environmental conditions, anatomical site, type of bone and orientation. In normal loading conditions, bones are subjected to either bending, torsion, compression or tension forces and often a combination. Trabecular and cortical bone will have different responses to different forces. For example, trabecular bone is stronger in compression than in bending. This is based on the structural arrangement of struts, which provide higher axial strength. Since vertebrae are more than half trabecular bone, vertebral compression tests provide significant information about this bone type.

In mechanical testing, a bone is loaded at a specified rate until failure. The deformation of the bone can be plotted as a function of load, which provides a failure deformation curve. From such a curve we can derive information including failure load, failure displacement, stiffness and energy to failure. We can combine these parameters with bone-specific geometric parameters to obtain a stress–strain curve. This provides material parameters including failure stress (strength), failure strain, normalized energy to failure (toughness) and the elastic modulus (rigidity). These mechanical properties are strongly influenced by the substructure of bone including bone structure and mineral content.

1.4.3 Assessment of Structure: Image Analysis

The term structure encompasses the amount, distribution and in the case of trabecular bone, the connectivity of bone. The amount of bone has been correlated with strength (McCalden et al., 1997; Thomsen et al., 2002). However, in trabecular bone, the size, spacing and orientation of individual trabeculae along with connectivity contribute to mechanical properties (Mosekilde, 1998; Garrahan et al, 1986). In postmenopausal osteoporosis, less connected trabecular bone increases fracture risk and this is also true in OVX rats (Kinney et al., 1998; Lane et al., 1999). In cortical bone, the distribution is

also important. For a given amount of bone, the distribution around the central axis influences mechanical strength.

Assessment of trabecular structure and connectivity relied on image analysis and strut analysis respectively. In image analysis, an image is taken of a two-dimensional bone surface and this image is then binarized to provide structural information including bone volume, bone thickness, trabecular separation and number. For strut analysis the image is then skeletonized to provide connectivity information such as the number of nodes, free–ends and joining struts (Serra, 1998; Grynpas et al., 1992; Garrahan et al., 1986). Decreased connectivity is characterized by a decrease in the number of node-node struts (Compston et al., 1993).

1.4.4 Assessment of Mineralization: Back Scattered Electron Imaging and Microhardness

Since bone is in a constant state of flux different packets of bone are at different stages of mineralization creating a distribution. This mineralization profile can be affected by age, disease and treatment.

Back scattered electron imaging is a method to obtain a mineralization profile. The bone surface is scanned in the scanning electron microscope and the electrons that are reflected almost directly back from the sample, the back scattered electrons, are collected. Since the probability of a collision increases with an increasing number of protons in the nucleus (atomic number), intensity of detected electrons is related to the atomic number of the constituents. Since calcium has the heaviest nuclei, the intensity of detected electrons is related to calcium concentration and similarly, the degree of mineralization.

Microhardness provides a link between mineralization and material properties. To assess hardness, an indenter is pressed into a material and the relationship between load and size of indent reflects resistance to penetration and similarly hardness (Amprino, 1961). In this manner, microhardness is defined as the resistance to penetration. Micro-

hardness has been shown to relate to mechanical properties and in particular the elastic modulus and yield strength (Evans et al., 1990; Currey and Brear, 1990). Microhardness has also been shown to correlate to the degree of mineralization (Carlstrom, 1954). This is based on the fact that mineral is hard compared to its collagenous matrix and therefore a bone with a higher degree of mineralization will be harder.

1.4.5 Assessment of Remodeling: Histomorphometry

Histomorphometry is a method for quantifying structural and remodeling parameters using histological sections (Erikson et al., 1994). Using a Goldner's Trichrome stained section we can differentiate between mineralizaed bone which stains green and nonmineralized bone (osteoid), which stains red. From this we can measure bone formation parameters including the osteoid volume, surface and thickness as well as the resorption parameter, the eroded surface although this is often difficult to decipher (Parfitt et al., 1987). Combining these parameters, we can get an overall assessment of remodeling. Histomorphometric analysis of OVX in the rat has shown an increase in both bone formation and resorption (Lane et al., 1999).

1.5 Growth Hormone

The human Growth Hormone (hGH) is a 22-kDa peptide hormone that is synthesized in the pituitary gland and stored in anterior pituitary cells (Goodman and Hirsch, 1968). It is a multifunctional protein hormone (Ogru et al., 2000) containing several discrete and functionally active domains (Ng, 1990). The hormone is biologically activated through binding to its receptor (Behncken and Waters, 1999).

GH has been shown to have significant effects on body composition (Brummer and Bengtsson, 1995). While growth is the most recognized function, GH also affects metabolism of major macromolecules such as proteins, carbohydrates and lipids. With respect to car-

bohydrates, GH treatment has been shown to impair insulin sensitivity thereby causing high blood glucose levels. This diabetogenic effect is a negative drawback of GH treatment (Cowell and Dietsch, 1995). With respect to proteins, GH stimulates amino acid uptake and protein synthesis and decreases protein oxidation (Copeland and Nair, 1994). Lipid effects include lipolysis and lipogenesis while skeletal effects include higher bone mass and growth although these effects will be discussed in more detail below. Overall, GH deficiency has been shown to cause dwarfism, increased obesity and low bone mass (Baroncelli et al., 2003). However, GH over–expression has been shown to cause gigantism and a bone disease called acromegaly (Kato et al., 2002).

1.5.1 Growth Hormone Structure

The GH molecule is a globular protein consisting of four anti–parallel α–helices (from residues 7–34, 75–87, 106–127 and 152–183), which are arranged in a left-twisted, tightly-packed helical bundle. The cysteine residues at amino acids 57 and 165 form a disulphide bridge that creates a large loop at the N–terminal region of the molecule. A disulphide bond between residues 182 and 189 forms a small loop at the carboxyl terminus (Ultsch et al., 1994).

This structure is thought to be important in binding to the growth hormone receptor (GHR). There are two binding sites on the GH molecule as determined through substitution studies (Cunningham et al., 1989). The first binding site consists of residues within helix 4 and to a lesser extent helix 1. The second binding site consists of residues within helix 3. However, binding of GHR to the first site is a prerequisite for binding to the second (De Vos et al., 1992). Once bound, GHR is dimerized and signal transduction via the JAK/STAT pathway occurs. It has been proposed that this mode of activation may not be unique since binding of GH isoforms, variants and fragments causes varying levels of downstream activity (Scanes and Campbell, 1995).

1.5.2 Effect of Growth Hormone on Adiposity

Growth hormone causes a reduction and redistribution of body fat and is therefore considered to be an integral player in lipid metabolism (Gertner, 1993; Heffernan et al., 2001; Effendi and Ng, 1993; Ho et al., 1996). In vivo experiments have been performed in both rodent and porcine models. Human effects are also understood since adult GH-deficient patients, have increased adiposity, which can be normalized with GH therapy (Jorgensen et al., 1994). In vitro studies have also been performed in which lipolysis is identified by the release of glycerol from adipose tissues while lipogenesis is measured as the rate of total lipid synthesis from exogenous glucose. Such studies show lipolytic (Heffernan et al., 2001; Moller et al., 1990; Richelson 1997) and antilipogenic effects (Moller et al., 1990; Richelson 1997). These effects have also been associated with an increase in fat oxidation (Heffernan et al., 2001). However, the mechanisms responsible are still in debate.

Dietz and Schwartz suggest that lipolysis occurs through action in the G protein signaling pathway in which there is an increase in hormone-sensitive lipase expression and phosphorylation (Dietz and Schwartz, 1991). Cell signaling after GHR homodimerizatoin results in the downstream activation of adenylyl cyclase and stimulation of cAMP production, which in turn stimulates hormone–sensitive lipase (Hollenga et al., 1991). Several groups have suggested that this signaling pathway has a role in chronic effects where as the protein kinase C pathway has a role in acute effects (Roupas et al., 1991; Kelly et al., 1994; Roupas and Herington., 1994). Protein kinase C has been shown to interact with membrane-bound GH receptors. This interaction causes receptor homodimerization and activation of the JAK/STAT pathway (Rue et al., 1997; Carter-Su., 1996; Costoya et al., 1999).

1.5.3 Skeletal Effect of Growth Hormone

A growth hormone deficiency causes stunted growth. However, exogenous GH treatment increases bone length, as well as the BMC and BMD of the lumbar spine and femoral neck. Although this effect is mostly seen in children it is also evident in adults (Gertner, 1993; Carrel and Allen, 2000). Growth is thought to occur directly by inducing the differentiation and proliferation of pre–chondrocytes in long bones (Issakson et al., 1985). Growth is also thought to occur indirectly through a systemic increase in IGF–I, which stimulates chondrocyte proliferation in chondrocyte columns (Ohlsson 2002; Isgaard et al., 1986). IGF-I has also been shown to stimulate osteoclasts through direct and indirect differentiation (Nishiyama et al., 1996; Kaji et al., 1997). Meanwhile, physiological levels of GH have been shown to stimulate osteoblastic proliferation and differentiation both in rat and human cells (Morel et al., 1993; Kassem et al., 1993).

Effect of Growth Hormone on the Rat Skeleton

The effects of hGH on the rat skeleton have been extensively studied. GH causes an increase in cortical bone formation of both young and old rats as shown through increases in BMD and cortical bone thickness (Andreassen et al., 1996; Andreassen et al., 1996; Jorgensen et al., 1991). Mechanical testing has also been performed, which shows an increased ultimate load when the femur is subjected to bending; however, there is no effect on stress or elastic modulus (Mosekilde et al., 1999). This absence of material effects is likely due to the observed increase in moment of inertia.

The effects of hGH have also been studied in OVX rats. Similar to the normal rats, GH increases cortical bone mass in aged OVX rats (Verhaeghe et al., 1996; Wang et al., 2001). Again, increased femoral load values were observed but not stress or elastic modulus (Andreassen and Oxlund, 2000; Mosekilde et al., 1998). Furthermore, the significant increases in femoral strength were only seen at GH doses greater than 2mg/kg/day (Mosekilde et al., 1998).

Histomorphic studies have shown a limited effect of hGH on trabecular bone. Eighteen month old rats were examined and showed no significant increase in trabecular bone volume, mineralizing surface, mineral apposition rate or bone formation rate (Gunness and Hock, 1995). This may, however, also be due to the age of the animals. Nevertheless, in younger sham rats treated with GH no significant increases were observed in vertebral or femoral neck strength (Andreassen et al., 1996).

1.5.4 Growth Hormone Peptides

Advances in peptide synthesis have made it possible to form specific and discrete functional domains, which have been associated with specific biochemical and physiological actions (De Laureto et al., 1995; Palidini et al., 1979; Chretien, 1999). For example, residues 1-43 have been associated with diabetes (Ng et al., 1974; Ridderstrale and Tornquist., 1996; Wroblewski et al., 1991). Similarly, the C-terminal region has been identified as the specific functional domain that controls lipid metabolism (Ogru et al., 2000; Bornstein et al., 1983; Wu and Ng 1993; Natera et al., 1994). Specifically, residues 177-191 encompass the minimum length that retains biological activity (Ogru et al., 2000; Heffernan et al., 2000). This peptide has been shown to have a similar action on adipose tissue as the intact hGH (Wijaya and Ng., 1993; McNeillie et al., 1982; Wu and Ng., 1993).

1.5.5 AOD9604

Due to the lipid metabolizing effects of the C-terminal domain of hGH residues ($hGH_{177-191}$), combined with the lack of a diabetogenic effect (Heffernan et al., 2001), this peptide is currently being considered as a potential anti-obesity drug (AOD). AOD is a cyclic peptide, cyclo(6,13)-H_2N–Leu–Arg–Ile–Val–Gln–Cys–Arg–Ser–Val–Glu–Gly–Ser–Cys–Gly–Phe–OH (Ogru et al., 2000). With the addition of tyrosine for stability, AOD is called AOD9604, which is the peptide currently under investigation. Structurally, AOD is similar to the intact hormone (Ogru et al., 2000).

Several studies have been performed to compare the AOD and hGH actions on lipid metabolism. Physiologically, they appear to have the same effect. AOD has been shown to decrease the body weight in an obese mouse (Heffernan et al., 2001). The peptide has also been shown to alter metabolic efficiency through an improvement in adipose tissue function or fatty acid metabolism (Natera et al., 1994). Furthermore, AOD reduces lipogenic activity (Ogru et al., 2000; Heffernan et al., 2000, Marcus et al., 1994; Wu and Ng., 1993) and increases lipolytic activity and fat-oxidation (Ogru et al., 2000; Heffernan et al., 2000; Heffernan et al., 2001; Marcus et al., 1994). However, while the effects of AOD and hGH appear to be similar, the time required to achieve them differs. The lipolytic effect of AOD was seen in minutes as opposed to the 4 hours that it took for hGH (Ogru et al., 2000; Wijaya and Ng., 1993). Wijaya and Ng have accounted for this discrepancy as the time required for post-translational activation of the hormone and the release of bioactive domains from the molecule to act on target tissues (Wijaya and Ng., 1993).

In addition to a change in rate of effect, the mechanisms also appear to differ. Although the binding site of AOD is unknown, it has clearly been shown in competition studies that it is not the GHR (Ogru et al., 2000, Heffernan et al., 2001; Ng et al., 2000). However, AOD appears to have the same downstream actions as hGH on lipid metabolism although it is mediated differently (Heffernan et al., 2000).

While the mechanism through which AOD affects lipid metabolism are largely unknown, there has been some indication that AOD9604 upregulates β_3–adrenergic receptors (β_3–AR), the major lipolytic receptors in rodent fat cells (Atgie et al., 1997). However, it has been shown that there is no direct mediation through the receptors, which opens the possibility of an indirect mechanism (Heffernan et al., 2001a).

1.6 Hypothesis and Objectives

In this study, we are testing the overall hypothesis that AOD9604 will prevent the ovariectomy–induced bone loss in a rat model of osteoporosis and will not affect the bone quality in normal rats.

The specific objectives of the study are:

1 To determine if AOD treatment prevents the effects of OVX on bone mass.

2 To determine if AOD treatment prevents the effects of OVX on bone mechanical properties.

3 To determine if AOD treatment alters the effects of OVX on bone structure and remodeling.

4 To determine if AOD treatment effects bone mineralization.

Chapter 2

Materials and Methods

2.1 Animal Care and Housing

This study involved 90 retired female breeder Sprague–Dawley rats, which were purchased from Harlan (Harlan Farms, Indiana) between 6 and 9 months of age. These rats were then housed at the animal facility of the Division of Comparative Medicine at the University of Toronto (Toronto, Ontario). After a 1–week acclimatization period, the veterinarians removed the ovaries (ovariectomized, OVX)of half of the rats. All operations were performed on the same day. The rats were then given identification ear–clips and were transferred into transparent plastic cages for the remainder of the study. The cages were lined with cornmeal bedding and contained a hide–away tube as well as an unlimited supply of tap water and lab chow. All of these cages were in the same room, which was monitored daily for temperature and humidity and the lights were set on a 12– hour on/off cycle. Furthermore, the rats were monitored throughout the entire study for any signs of illness or stress.

2.2 Drug Preparation and Administration

Two separate drug doses were used: 0.25 mg/kg/day and 0.5 mg/kg/day. These weight–based dosages were achieved by weighing the rats every two weeks and adjusting concentrations accordingly. The drug was reconstituted daily by weighing the peptide powder and adding distilled water to achieve the calculated concentration. When the powder fully dissolved it was injected into sterile vials using a syringe.

The vials were brought to the veterinary technicians at the Division of Comparative Medicine at the University of Toronto (Toronto, Ontario) who administered the solution by gavages. Doses were given 5 days a week over a period of 12 weeks. All rats were rewarded with a fruit loop.

2.3 Experimental Design

2.3.1 Treatment Groups

This study was designed to test two different doses of AOD (0.25 and 0.5 mg/kg/day) in both OVX and normal skeletons. To achieve this, the 90 rats were divided into 6 groups of 15 as shown in Table 2.1.

2.3.2 Experimental Timeline

The study was timed to provide acclimatization, a 12 week dosing period for treatment groups and weight–based AOD concentrations as shown in Figure 2.1.

2.3.3 Sacrifice and Dissection

Following the 12 week treatment period, each rat was euthanized via exsanguination in a CO_2 chamber and this was followed by cervical dislocation. Treatment groups were

Model	Group	Abbreviation	Number of Rats	Dose (mg/kg/day)
Normal	Control	NC	15	0
Normal	AOD–0.25	N(0.25)	15	0.25
Normal	AOD–0.5	N(0.5)	15	0.5
OVX	Control	OC	15	0
OVX	AOD–0.25	O(0.25)	15	0.25
OVX	AOD–0.5	O(0.5)	15	0.5

Table 2.1: Treatment groups and AOD dosages

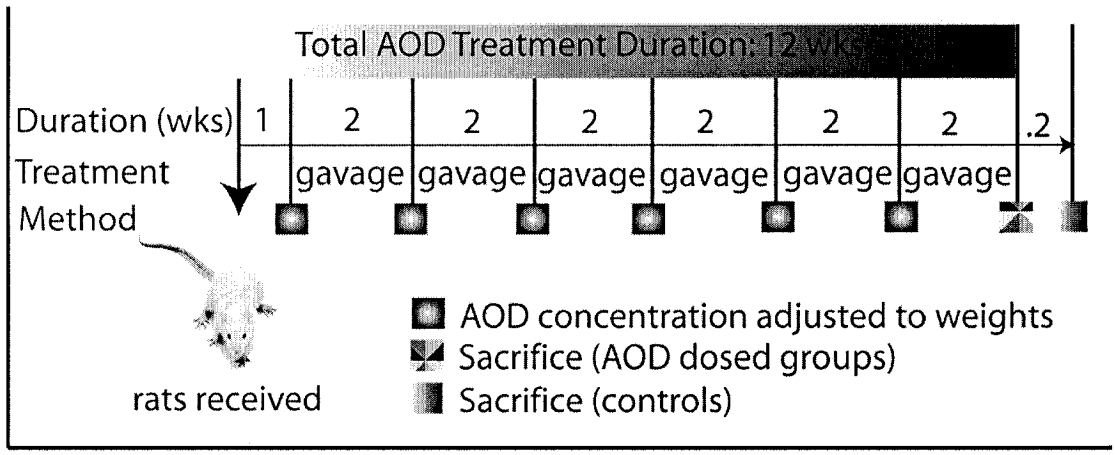

Figure 2.1: Experimental timeline

sacrificed exactly at the 12 week point and the control groups were sacrificed two days later due to time constraints (Figure 2.1).

Immediately after sacrifice, the spines along with the femurs and the left tibiae of each rat were roughly excised and inserted into pre-labeled plastic tubes for further processing. These tubes were then placed onto a bed of ice after which they were transferred to a freezer maintained at (-20°C). The right tibiae were dissected and fixed in 70% ethanol.

2.4 Assessment of Bone Quality

2.4.1 Dual Energy X–ray Absorptiometry

Dual Energy X–ray Absorptiometry (DXA) measures the bone mineral content and bone mineral density. Tests were performed on the left femurs and lumbar vertebrae (4–6).

Sample Preparation

The excised and cleaned left femurs and lumbar vertebrae (4–6) were removed from the freezer and kept on a bed of ice prior to testing.

Machine Set–up

DXA was performed using the PIXImus Densitometer (Lunar GE Corp.), which is a DXA machine specifically designed for small animal bones. Before performing measurements, the machine was calibrated. This involved placing a standard aluminum/lucite plate in the scanning area and running a calibration scan.

Tests

Bones were placed in the desired configuration on a polystyrene plate that simulates soft tissue thickness on bone. Femurs were placed individually on the plate caudal side down and vertebrae were also placed caudal side down but in a row of three to simulate the natural arrangement in the skeleton. Scans were then run and the software generated bone mineral density (BMD) and bone mineral content (BMC) values.

Follow–up

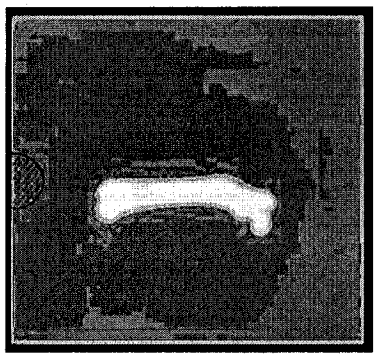

Figure 2.2: DXA scan of the projected area of the femur

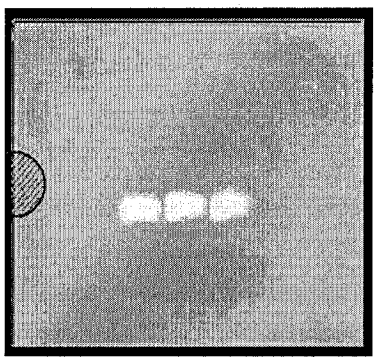

Figure 2.3: DXA scan of the projected are of the vertebra

Following testing, the bones were re–wrapped in saline soaked gauze and returned to the freezer for future mechanical tests (torsion testing).

Analysis

Values were determined based on the entire projected bone area as depicted in Figure 2.2 and figure 2.3.

2.5 Assessment of Mechanical Properties

Four mechanical tests were performed during this study: three point bending, torsion, femoral neck fracture and vertebral compression. Tests were chosen based on the type of bone they test (cortical vs. trabecular), loading conditions and clinical relevance.

2.5.1 Three Point Bending

Three point bending tested the cortical bone of the right femur in bending.

Sample Preparation

Femurs were removed from the freezer two hours prior to testing to ensure thawed samples. During this transition period, the bones were kept moist with saline solution. Meanwhile, each femur was measured using digital calipers and a mark was placed at the mid-section of the bone using a waterproof marker.

Machine set–up

Tests were performed on a mechanical testing machine (Instron 4465, Instron Canada Inc.) with a 1000N load cell and a testing jig. This jig consisted of an indenter that was attached to the load cell and two supports placed 15.6 mm apart (Figure 2.4 a). Once the test jig was inserted into the load cell, the machine was balanced.

Tests

Bones were individually placed on the jig supports with the cranial side facing upwards as depicted in Figure 2.4 a. Bones were then preloaded to approximately 1.0 N after which tests were run at 1mm/min until failure. The test data was collected from the Instron machine using Lab View data acquisition software (National Instruments Corp.; Austin, TX).

Follow–up

Immediately after testing, the proximal end of the femur was re–wrapped in saline soaked gauze and replaced into the plastic test tubes in the freezer for further testing (femoral

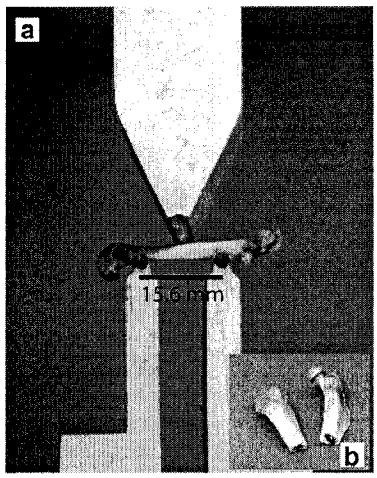

Figure 2.4: Three Point Bending: a) bone placement in apparatus b) bending fracture

neck fracture). The distal end was embedded in epoxy for SEM imaging and normalization as discussed below.

Unnormalized Data Analysis

The time data obtained from the test was converted into displacement data using the test speed (1mm/min). This was used to create a load–displacement curve with spreadsheet software (Excel2000, Microsoft). From this curve, unnormalized mechanical properties (failure load, failure displacement, stiffness and energy to failure) were determined as outlined in Figure 2.5.

Epoxy Embedded Femurs

The distal end of the right femur was pressed into Fimo (Fimo Classic, Eberhard Faber) such that the fracture surface faced upwards. The Fimo and femur combination was then placed in an embedding mold along with an ID tag (Figure 2.6 b). Epoxy was then poured into this mold and left to harden for 48 hours. The hardened blocks were then sliced, using a low speed saw (Isomet, Bueler), as close to the fracture surface as was possible while still maintaining the full cross-section of the bone (Figure 2.6 c).

Normalizing Three Point Bending Data

The epxoy embedded femur blocks were secured onto a plastic plate using Fimo (Fimo,

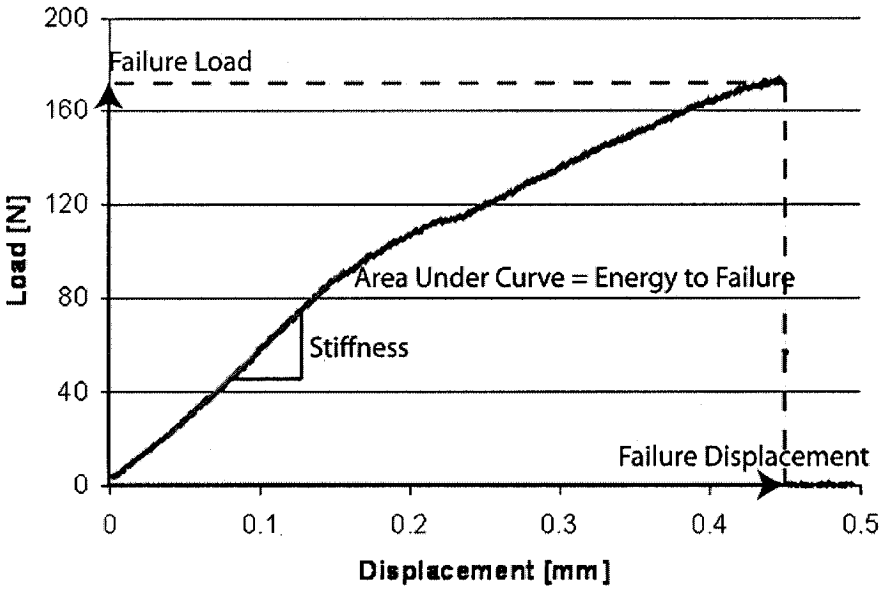

Figure 2.5: Determination of three point bending unnormalized properties

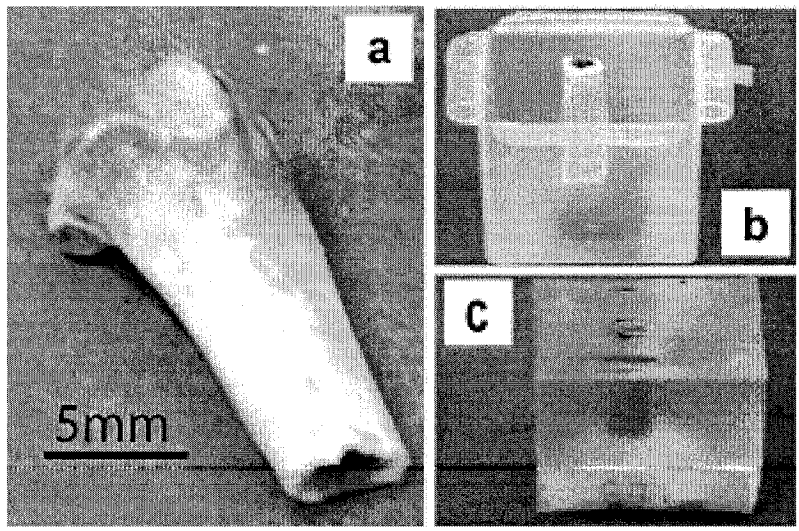

Figure 2.6: Embedding the distal end of the right femur in epoxy

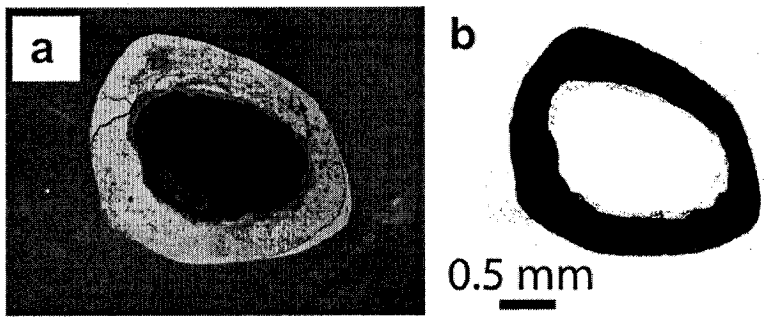

Figure 2.7: Imaging the femoral fracture surface a) SEM image b) binarized image

Eberhard) and carbon taped and carbon coated. Backscattered images were then obtained using the scanning electron microscope (Figure 2.7 a). These images were binarized using image analysis software (ImageJ 1.28u, National Institute of Health; Figure 2.7 b).

Normalized Data Analysis

The moment of inertia and diameters were obtained from the binarized image and these parameters were used to convert the unnormalized parameters into normalized parameters (failure stress 2.1, failure strain 2.2, elastic modulus 2.3, normalized energy to failure 2.4; Turner and Burr, 2001).

$$\text{Failure Stress (MPa)} = \frac{M_f d_1}{2I} \tag{2.1}$$

M_f: Bending moment (N·mm)

d_1: Anterior–Posterior diameter (mm)

I: Elliptical moment of inertia (mm^4)

$$\text{Failure Strain (\%)} = \frac{6d_1\delta_f}{l_o^2} x100 \tag{2.2}$$

d_1: Anterior–Posterior diameter (mm)

δ_f: Failure displacement (mm)

l_o Gauge length (mm)

$$\text{Elastic Modulus (MPa)} = \frac{kl_o^3}{48I} \tag{2.3}$$

k: Stiffness (N/mm)

l_o: Gauge length (mm)

I: Elliptical moment of inertia (mm^4)

$$\text{NEF} = \sum_{j-1}^{n}(\sigma_{j-1})(\epsilon_{j-1} - \epsilon_j) + \frac{(\sigma_{j-1} - \sigma_j)(\sigma_{j-1} - \sigma_j)}{2} \tag{2.4}$$

NEF: Normalized Energy to Failure (mJ/mm^3) σ: Stress (MPa)

ϵ: Displacement (mm)

n: Total number of data points to yield

j: Integer Increments from 1 to n

2.5.2 Torsion Testing

Torsion testing assessed the cortical bone of the left femur loaded in torque.

Sample Preparation

Femurs were removed from the freezer 2 hours before testing to allow them to thaw. During this period, the bone length was measured using digital calipers and the midpoint was marked with a waterproof marker. The extremities of the femur were removed using a low speed saw (Isomet, Bueler). A 16 mm gauge length was then marked on the severed bone and a 16 mm strip of saline soaked gauze was wrapped around the gauge length (Figure 2.8a). The gauze remained on the bone until testing and was kept moist with saline at all times.

The bone was then secured within two bolt heads using a customized jig. To achieve this, the wrapped bone was first placed vertically into a bolt head and secured with polymethyl methacrylate (PMMA) (Figure 2.8 b). The PMMA was allowed 10 minutes to dry before the bone-bolt assembly was inverted (Figure 2.8 c). Beneath this inverted assembly, a second bolt was placed and nuts were used to fix it at the required height and position. The lower bolt head was filled with PMMA and the inverted bolt–bone assembly was screwed down so that the remaining free end was secured in PMMA (Figure 2.8 d). The PMMA was allowed 10 minutes to dry before the bolt–bone-bolt assembly as removed from the jig.

Machine Set–up

Tests were performed on a custom built machine, which consisted of one stationary and one rotating chuck along with a 20in–lb load cell and a gauge to measure the angle of rotation (Figure 2.9a). The load was verified for accuracy before testing.

Testing

The bolt–bone–bolt assembly was carefully secured into the chucks as shown in Figure 2.9a. The gauze was removed immediately before testing. Tests were run at approximately 0.7 rad/min until failure. Time, rotation and torque data were acquired by LabView data acquisition software.

Analysis

Torque was plotted against angle of rotation using spreadsheet software (Excel2000, Mi-

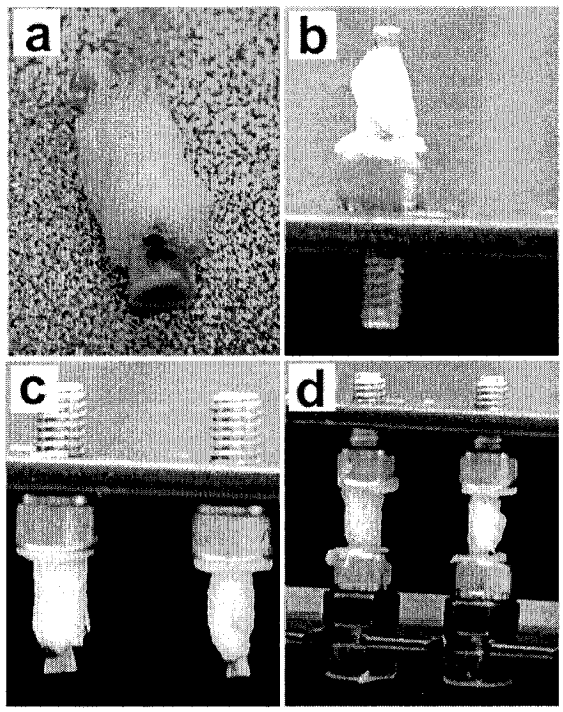

Figure 2.8: Bone preparation for torsion testing a) gauze wrapped bone b) bone placement in bold c) inverted bolts d) bone–bolt–bone assembly

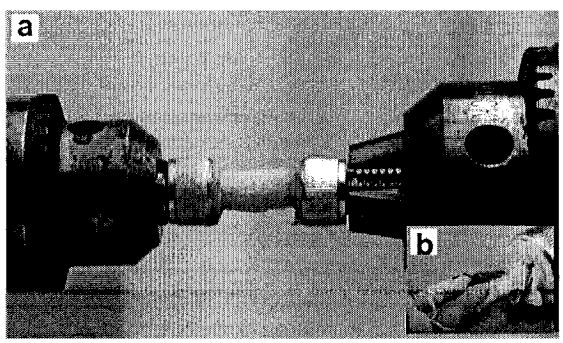

Figure 2.9: Torsion Testing a) bone placement in apparatus b) torsion fracture

crosoft). From this curve, unnormalized mechanical properties (failure torque, angular deformation at failure, stiffness and energy to failure) were determined as outlined in Figure 2.10.

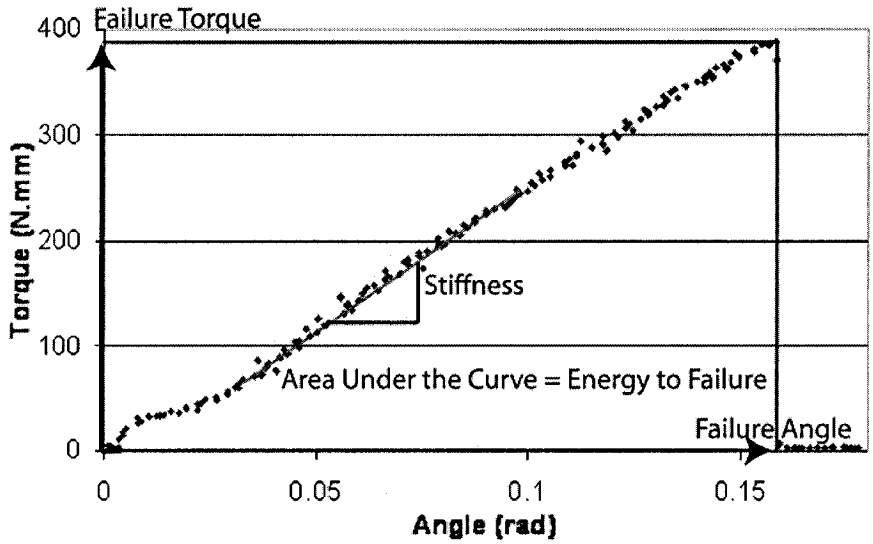

Figure 2.10: Determination of unnormalized mechanical properties in torsion

The large diameter and the polar moment of inertia were obtained from the epoxy embedded femurs using image J analysis as outlined in §2.5.1 The polar moment of inertia and large diameter were used to convert the unnormalized parameters into normalized parameters (failure shear stress 2.5, failure shear strain 2.6, shear modulus 2.7, normalized energy to failure 2.8; Turner and Burr, 2001).

$$\text{Failure Shear Stress (MPa)} = \frac{T_f a}{2J} \tag{2.5}$$

T_f: Failure Torque (N·mm)

a: Large diameter of femur (mm)

J: Polar moment of inertia (mm^4)

$$\text{Failure Shear Strain (\%)} = \frac{a\alpha_f}{2l_o}100 \tag{2.6}$$

a: Large diameter of femur (mm)

α_f: Failure rotation (mm)

l_o: Gauge length (mm)

$$\text{Shear Modulus (MPa)} = \frac{sl_o}{J} \tag{2.7}$$

s: Stiffness (N·mm/rad) or (mJ/rad)

l_o: Gauge length (mm)

J: Polar moment of inertia (mm^4)

$$\text{NEF} = \sum_{j-1}^{n}(\tau_{j-1})(\gamma_{j-1} - \gamma_j) + \frac{(\tau_{j-1} - \tau_j)(\tau_{j-1} - \tau_j)}{2} \tag{2.8}$$

NEF: Normalized Energy to Failure (mJ/mm^3)

τ: Shear stress (MPa)

γ: Shear strain (mm)

n: Total number of data points to yield

j: Integer increments from 1 to n

2.5.3 Femoral Neck Fracture

Femoral neck fracture tests the cortical and trabecular bone of the femoral neck in both compression and tension modes. While this test is clinically relevant, only unnormalized

analysis is available due to the complex geometry of the neck region as well as the complex loading condition.

Sample Preparation

Samples were removed from the freezer two hours before testing to ensure that they were thawed. Immediately before testing, the samples were secured into a testing jig. This jig consisted of a stainless steel tube with a hole bored into it for the bone to sit in and set screws to hold the bone vertical during set–up. Loading the bone into this jig piece first involved greasing the jig chuck with Vaseline and placing a square of cardboard in the base to simplify removal. The bone was then placed in the jig with the severed side down and the four screws were tightened to secure the bone in position. Following this, PMMA was pressed into the jig chuck surrounding the bone to tightly seal it. The PMMA was left to dry for 10 minutes prior to testing and during this period the bone was covered in saline soaked gauze. Meanwhile, the distance between the edge of the PMMA and the top of the femoral head was measured using digital calipers and the value was recorded.

Machine Set–up

The femoral neck fracture tests were performed on a mechanical testing machine (Instron 4465, Instron Canada Inc.) with a 1000N load cell. The jig containing the bone was secured to the load cell and the machine was calibrated and balanced. A plate with a hole drilled out of it was placed beneath the top jig in a position that would facilitate contact only between the plate and the femoral head as shown in Figure 2.11.

Tests

Each bone was preloaded to approximately 1N. The tests were then run at 2.5 mm/sec until femoral neck fracture.

Analysis

The time data obtained from the test was converted into displacement data to create a load-displacement curve using spreadsheet software (Excel2000, Microsoft). From this curve, unnormalized mechanical properties including ultimate load, failure deformation,

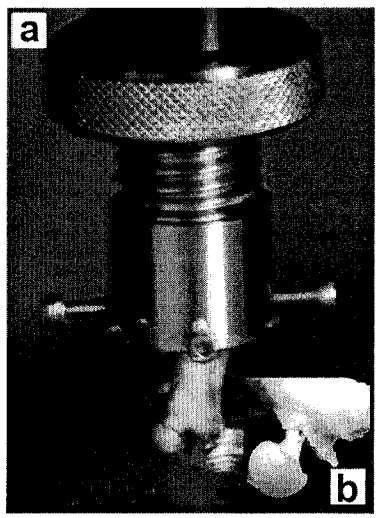

Figure 2.11: Femoral neck fracture testing a) bone arrangement in apparatus b) Femoral neck fracture

energy to failure and stiffness were determined as shown in Figure 2.12.

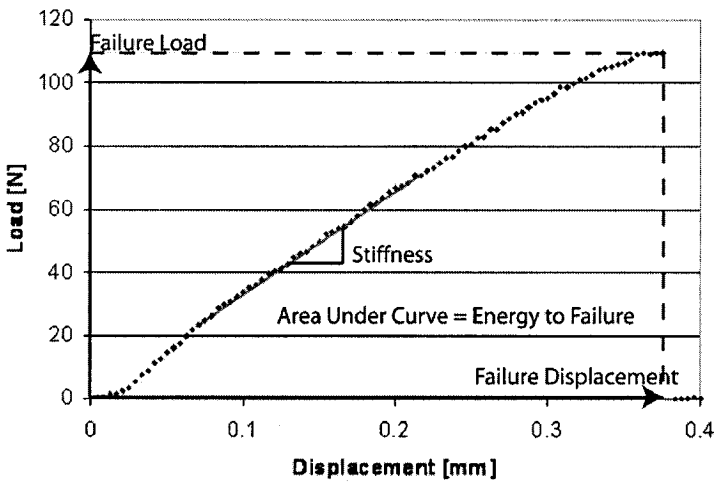

Figure 2.12: Determination of unnormalized mechanical properties in femoral neck fracture

2.5.4 Vertebral Compression

Vertebral compression tested the trabecular bone of the 4th lumbar vertebrae in compression.

Sample Preparation

Samples were removed from the freezer 2 hours prior to testing and maintained in saline soaked gauze. While thawing, both the medial–lateral diameter and cranial–caudal diameter at mid–shaft were measured and recorded. Once thawed, vertebrae were secured vertically into individual bolt heads using PMMA. PMMA was allowed to set for a minimum of 10 minutes and the bone was kept moist with saline soaked gauze throughout this period and up until testing. Before testing, the gauge length was recorded, which was measured as the distance from the edge of the PMMA to the end of the bone minus 2.5 mm.

Machine Set–up

Vertebral compression tests were performed on a mechanical testing machine (Instron 4465, Instron Canada Inc.) with a 1000N load cell. A stainless steel plate containing 19 holes, each 2.5 mm deep and differing 0.1 mm in diameter was placed beneath the load cell as shown in Figure 2.13 a. The purpose of this plate was to provide a tight fit with the distal end of each vertebra to prevent lateral movement and consequent shear forces on the bone. The desired hole was selected individually for each bone after which the bone-containing bolt was screwed into a connector on the load cell and the hole was clamped in place directly beneath the bone. The machine was then rebalanced.

Tests

The vertebrae were loaded to 5 N to ensure contact on all sides of the hole as well as the bottom of the plate. Tests were then run at 1mm/min until failure, which was defined as a 10% drop in force. Load versus time data was acquired from the Instron by LabView data acquisition software.

Analysis

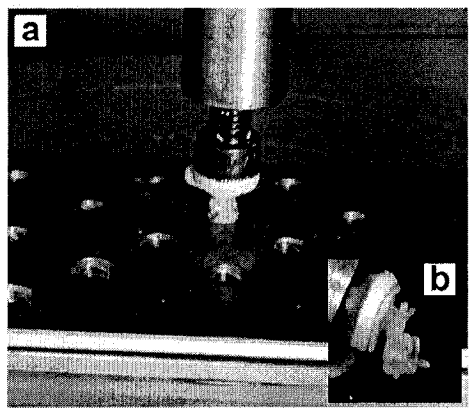

Figure 2.13: Vertebral Compression a) bone arrangement in apparatus b) Fracture

Time data was converted into deformation data to construct a load–deformation curve from which unnormalized properties (failure load, failure deformation, stiffness and energy to failure) were determined as shown in Figure 2.14. The cross-sectional area at mid-point (determined from mid-point diameters 2.13 and the gauge length) were used to obtain normalized data based on the equations derived from Turner and Burr (Turner and Burr, 2001; failure stress 2.9, failure strain 2.10, elastic modulus 2.11, normalized energy to failure 2.12.

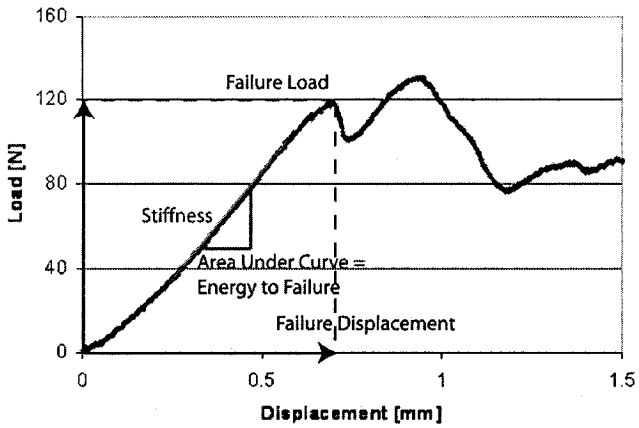

Figure 2.14: Determination of unnormalized mechanical properties in vertebral compression

$$\text{Failure Stress (MPa)} = \frac{F_f}{A_{cs}} \tag{2.9}$$

F_f: Bending moment (N·mm)

A_{cs}: Cross-sectional area (mm^2)

$$\text{Failure Strain (\%)} = \frac{\delta_f}{l_v} 100 \tag{2.10}$$

δ_f: Failure displacement (mm)

l_v Gauge length (mm)

$$\text{Elastic Modulus (MPa)} = \frac{k l_v}{A_{cs}} \tag{2.11}$$

k: Stiffness (N/mm)

l_v: Gauge length (mm)

A_{cs}: Cross-sectional area (mm^2)

$$\text{NEF} = \sum_{j-1}^{n} (\sigma_{j-1})(\epsilon_{j-1} - \epsilon_j) + \frac{(\sigma_{j-1} - \sigma_j)(\sigma_{j-1} - \sigma_j)}{2} \tag{2.12}$$

NEF: Normalized Energy to Failure (mJ/mm^3)

ϵ: Displacement (mm)

n: Total number of data points to yield

j: Integer Increments from 1 to n

$$\text{Cross–sectional Area (mm}^2) = \pi \frac{d_{ml} d_{cc}}{4} \tag{2.13}$$

d_{ml}: Medial-lateral diameter (mm)

d_{cc}: Caudal-cranial diameter (mm)

2.6 Assessment of Bone Formation, Structure and Connectivity

2.6.1 Histomorphometry

Histomorphometry provides parameters of bone formation and resorption along with bone structure.

Sample Preparation:

Spurr Embedded Tibia

The right tibiae that had previously been fixed in 70% ethanol were coronally and transversely sectioned using a low speed bone saw (Isomet, Bueler). Proximal cranial sections were then inserted into individual cassettes and placed in 70% ethanol for an additional week. Following this, sections were dehydrated and spurr embedded following a modified procedure that was developed in the special histology lab at Mount Sinai Hospital (An et al., 2003). Dehydration involved placing the cassettes in increasing amounts of acetone (70%, 90%, 100%, 100%) for 3 to 4 days at each step. This dehydration process was accelerated by placing samples under a vacuum. The samples were then infiltrated with increasing percentages of spurr resin (50%, 80%, 100%, 100%) while acetone comprised the remainder of the solution. This infiltration process was also performed under a vacuum. Samples were then removed from the 100% spurr resin and placed inferior side

down in the center of an embedding mold along with an identification tag. The molds were then filled with spurr resin and placed in a 50°C oven for 48 hours to cure the spurr.

Slide Preparation

The spurr embedded tibiae blocks were sectioned using a semi–automatic microtome (Reichert–Jung 2050). Three sequential 5μm sections were taken from each block and placed in a 60°C waterbath that contained a small quantity of gelatin. Sections were then placed on gelatinized slides and a piece of plastic was placed on top of the section and air–bubbles were carefully smoothed out. A siliconized slide was placed on top of the plastic piece to protect the section resting beneath. All slides from an individual block were stacked, clamped together and placed in a 65°C oven for 48 hours.

Goldner's Trichrome Stain

The second 5μm section slide was stained using Goldner's Trichrome following the standard procedure (Schenk et al., 1994). Slides were hydrated by dipping in descending concentrations of ethanol (100%, 95%, 70%) followed by tap water and then distilled water. Slides were then left in Weigert's Iron Hematoxylin for 15 minutes before rinsing 4 times with distilled water. Following this, slides were left in running tap water for 15 minutes and then rinsed twice in distilled water. Slides were then left in Ponceau Acid/ Fuchsin, Phosphomolybdic Acid, Orange G and 1% Light Green for 15, 8 and 15 minutes respectively and between each solution, slides were dipped twice in 1% acetic acid. Finally, slides were cleaned in ethanol, dehydrated in xylene and coverslipped using permamount. The Goldner's Trichrome stained slides were placed in the microscope sample holder.

Machine Set–up

A Zeiss microscope attached to a video camera (Retiga 1300) acquired the image, which was then analyzed by Bioquant morphometry program computer software (Bioquant Nova Prime, version 6.50.10). Magnification was set at 100X. A sample slide was first analyzed for calibration.

Testing

A ten field area ($10mm^2$) was tested on each bone. This area was selected three quarters of a millimeter down from the growth plate and half a millimeter away from the cortical bone on each side to ensure that the measurements included trabecular bone only rather than the intermediary zone. Parameters were measured by selecting appropriate thresholds based on the fact that mineralized bone stained green and osteoid stained red.

Analysis

Analyzed parameters included: osteoid volume, osteoid surface as well as the combined parameter osteoid volume divided by bone volume as shown in Figure 2.15

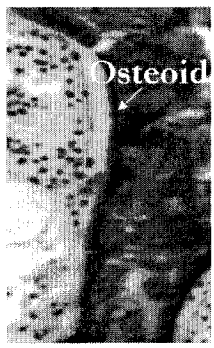

Figure 2.15: Identification of bone formation parameters from histomorphometry: Osteoid Volume and Osteoid Surface

2.6.2 Image Analysis

Image analysis is used to determine both the architecture and connectivity of trabecular bone struts.

Sample Preparation

Epoxy Embedded Tibia

The left tibia was dissected and sectioned transversely. The proximal end was cleaned and marrow was removed. Tibias were then coronally sectioned and the cranial sections were placed in individual plastic cassettes. The cassettes were placed in 70% acetone to

dehydrate the bone and then the bones were left in a room temperature fume hood for 12 hours to completely dry. After drying, bones were placed cut–side down in embedding molds and epoxy was poured over top. The bone–embedded epoxy blocks were then left to dry for 48 hours before removing the mold. In order to expose the bone, a thin section was removed from the surface using a semi–automatic microtome (Reichert–Jung 2050). Epoxy embedded tibia were used for image analysis. The blocks were secured with Fimo (Fimo, Eberhard) onto a plastic plate, wrapped in carbon tape and carbon coated.

Machine Set–up

Samples were imaged on a Hitachi S-2500 (Nissei Sangyo America Ltd., Rolling Meadows, IL) scanning electron microscope. The accelerating voltage was 20 kV; the spot size was 7; the working distance was 15mm and the scan speed was 16.7 ms/484 lines.

Testing

Images were taken of the trabecular bone area beneath the growth plate at 50 X magnification. A pixel to measurement parameter was determined.

Analysis

In the images, mineralized bone appeared grey or white while the unmineralized bone and epoxy appeared black. These images were analyzed on a Quantimet 500 IW system using the program Quips, written by Dr. Dumitriu. Within a chosen area of analysis, the program identified structural parameters including trabecular bone volume, trabecular thickness, trabecular number and trabecular separation. Connectivity parameters including total length of connected bone, nodes, free ends, node–node struts, node–free end struts and free–free struts as shown in Figure 2.16 were also determined.

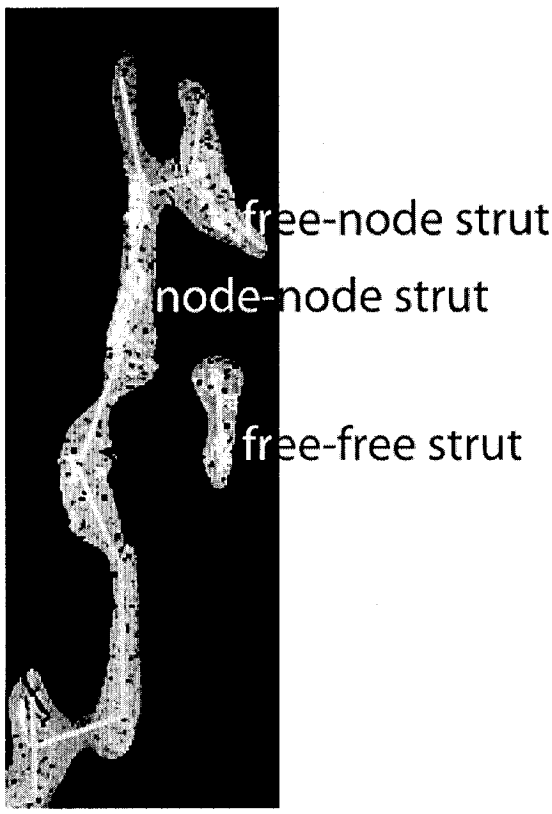

Figure 2.16: Identification of node–node, free–node and free–free struts

2.6.3 Femoral Cross-Section Geometry

The binarized images from the femur that were used in three point bending normalization §2.5.1 were also used to determine the diameters and thicknesses at midshaft.

2.7 Assessment of Mineralization

2.7.1 Backscattered Electron Imaging

Sample Preparation

The spurr embedded tibiae, which had previously had sections removed for histomorphometry analysis, were prepared for backscattered electron imaging (BSE). The surface

of each block was ground on 600 grade grinding paper followed by 1200 grade. Blocks were then polished using 6 μm and then 1 μm diamond polish. This process has previously been described (Grynpas et al. 1994). The blocks were then mounted on a plastic plate using Fimo (Fimo, Eberhard) and this assembly was wrapped in carbon tape and coated with carbon. An aluminum standard was also affixed.

Machine Set–up

BSE was performed in a scanning electron microscope. The accelerating voltage was 20 kV; the spot size was 7; the working distance was 15mm and the scan speed was 16.7 ms/484 lines.

Testing

Before imaging each specimen, the signal was calibrated using an aluminum standard. Brightness was adjusted to approximately 150 and pixel count to 20, 000. Cortical and trabecular bone of the specimens were imaged in four fields. After imaging each specimen, the signal was re–calibrated using the aluminum standard to ensure no beam fluctuation (Boyce et al. 1990). In the event of fluctuation, the signal was re–calibrated, the image was re–taken and the signal was checked again.

Follow–up

Blocks were removed from the plates in preparation for microhardness testing.

Analysis

Images of each field were stitched together for analysis of the whole section. An example of the resulting image is shown in Figure 2.17. Masks were created over this base image to isolate cortical and trabecular regions. Both the spur resin and the unmineralized bone appeared black. The grey sections reflected bone with varying degrees of mineralization where dark grey represented low mineralization and white represented a high degree of mineralization. This was quantified on a Quantimet 500 IW system using the program Quips, written by Dr. Dumitriu. The program set up a series of bins based on intensity and calculated the number of pixels falling in each bin. From this information,

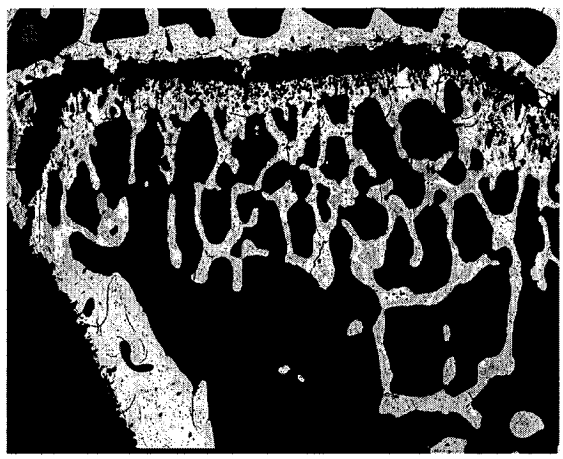

Figure 2.17: BSE image for mineralization analysis

a histogram of area as a function of intensity was created for each image. From these histograms the maximum peak height, the width at half of the maximum height, the grey level at maximum peak height and the logit function were determined. The width at half of the maximum height reflects the distribution of mineral while the grey level at maximum peak height reflects the mineral concentration. Meanwhile the logit function provides information about the shape of the curve. To determine the value for the logit function an arbitrary cut–off was determined and the logit is the natural logarithm of the area under the curve to the right of the cut–off over the area under the curve to the left of the cut–off line (Bracci et al., 1998).

2.7.2 Microhardness

Trabecular and cortical bone hardness of the right tibia were determined.

Sample Preparation

The spurr embedded tibiae, which were previously polished to 1 μm diamond finish and used for BSE, were hardness tested. These blocks were secured onto a small plastic Petri dish using Fimo.

Machine Set–up

Testing was performed on a Mitutoyo HM–122 microhardness tester (Mitutoyo, Japan) with a Vickers diamond indenter. The machine was zeroed before each test.

Testing

The dish containing the block was secured into the sample holder of the microhardness tester. Under a magnification of 20X the sample was aligned such that the point of interest would be directly under the indenter. Care was taken to avoid placement over cracks, edges, polishing scores and other imperfections. Once aligned, the specimen was indented with a load of 25g for 10s. The lengths of the indentation's two diagonals were then measured. 10 indents were made on the cortical bone (5 lateral, 5 medial) and 10 indents were made on separate trabeculae.

Analysis

Average cortical and trabecular hardness were determined using the equations: 2.14 and 2.15.

$$\text{Vickers Hardness (HV)} = \frac{F}{gS} \tag{2.14}$$

F: Test Force (N)

G: Acceleration due to gravity (9.8m/s^2)

S: Surface area of indentation (mm^2)

$$\text{Surface Area of Indentation (mm}^2\text{)} = \frac{1.854w}{D^2} \tag{2.15}$$

w: Test weight (g)

D: Average length of two diagonals (mm)

2.8 Statistical Analysis

Statistical analysis was performed using statistical software, SPSS (version 12.1). Comparisons involving two groups were performed using an independent t–test. Multiple comparisons were performed using a one–way ANOVA with the pairwise comparison Protected Fisher's Least Significant Difference (LSD) post hoc test. A p–value less than 0.05 was considered significant while a p–value less than 0.1 was considered a trend. Damaged samples and extreme outliers (three standard deviations from the mean) were excluded from the analysis. All data is displayed as mean $\pm$ standard error of the mean (SEM).

Chapter 3

Results: The Skeletal Effect of OVX

The results have been divided into three sections. The first focuses on the skeletal effect of OVX in the absense of AOD, the second focuses on the skeletal effect of AOD in the absense of OVX and the third focuses on the combined effect of the treatments. This is to provide proper controls and comparisons for the hypothesis.

3.1 Introduction

This chapter examines the effect of reduced estrogen, as a result of ovariectomy, on the rat skeleton. Since the OVX rat is a control for the state of extreme bone loss and high fat mass, it is important to ensure its functionality and also to isolate the effects that are due to OVX. For the sake of clarity as well as consistency with the other results chapters, this chapter is divided into the effect of OVX on body weight, cortical bone and trabecular bone. All data is expressed as mean $\pm$ standard error of mean (SEM) and ^{a} reflects a significance of $p<0.05$ vs. normal control while ^{b} reflects a significance of $p<0.1$ vs. normal control.

Group	Initial Weight (g)	Final Weight (g)	Weight Gained (%)	n
NC	339.1 ± 8	343.9 ± 11	1.4 ± 2	13
OC	316.9 ± 7	382.3 ± 5	21.2 ± 2[a]	15

Table 3.1: Body weight of normal and OVX rats.

[a]reflects a significance of $p<0.05$ vs. NC

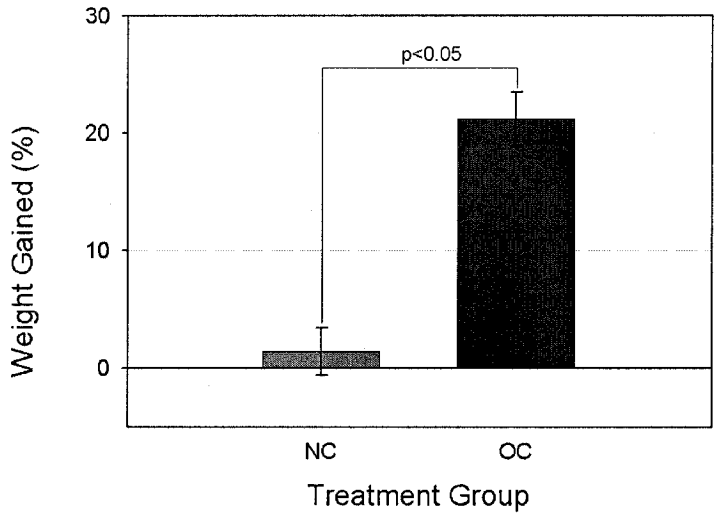

Figure 3.1: Percentage of body weight change: comparing normal and OVX rats.

3.2 The Effect of OVX on Body Weight

The normal control group was heavier than the OVX controls at the commencement of the study so we can only compare the percentage of weight gained (Table3.1). From this parameter, as shown in Figure 3.1, normal controls gained only 1.4% of original body weight while the OVX controls gained a highly significant 21.2% ($p<0.001$). Clearly, OVX induced the expected weight gain.

3.3 The Effect of OVX on Cortical Bone

3.3.1 Bone Mineral Density: DXA

The effect of OVX on bone mineral density (BMD) and bone mineral content (BMC) was analyzed using Dual Energy X–Ray Absorptiometry (DXA). In the cortical bone of the left femur, the OVX controls had a significantly lower BMD compared to the normal controls ($p<0.05$; Figure 3.2; Table 3.2). This shows that OVX decreased the amount and density of cortical bone.

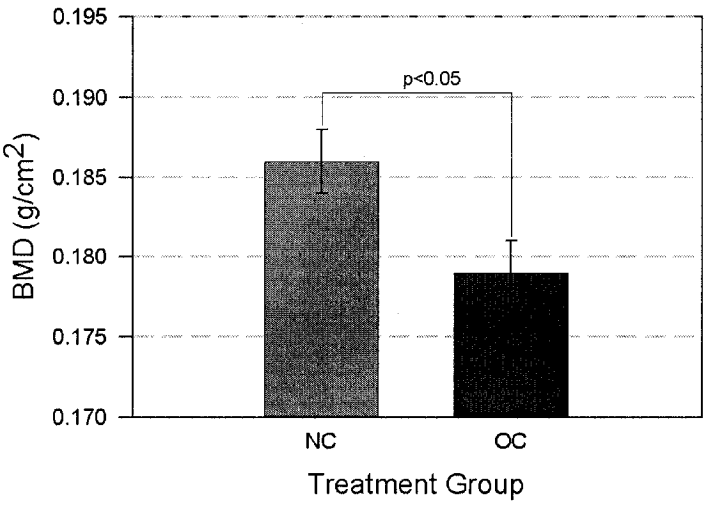

Figure 3.2: Bone Mineral Density (BMD) of the left femur: comparing normal and OVX rats.

Group	BMD (g/cm^2)	BMC (g)	n
NC	0.186 ± 0.002	0.503 ± 0.009	15
OC	0.179 ± 0.002^a	0.495 ± 0.009	14

Table 3.2: Femoral BMD and BMC of normal and OVX rats.

[a]reflects a significance of $p<0.05$ vs. NC

3.3.2 Mechanical Properties

Cortical bone mechanical properties were determined through three point bending and torsion tests. The right and left femurs were used respectively.

Three-point bending

There were no significant differences in the unnormalized mechanical properties, including failure load, failure displacement, energy to failure and stiffness (Table 3.3). However, there was a decreasing trend ($p<0.1$) in the failure stress of OVX controls compared to normal controls, which indicates a decrease in strength (Table 3.4).

Group	Failure Load (N)	Failure Displacement (mm)	Energy to Failure (mJ)	Stiffness (N/mm)	n
NC	159.4 ± 4.8	0.55 ± 0.02	57.0 ± 4.1	566.1 ± 21.9	14
OC	146.6 ± 6.8	0.63 ± 0.04	60.6 ± 4.5	522.3 ± 22.8	13

Table 3.3: Three point bending of normal and OVX rat femurs (unnormalized data).

Group	Failure Stress (MPa)	Failure Strain (mm/mm)	Energy to Failure (MPa)	Elastic Modulus (MPa)	n
NC	130.6 ± 5.2	0.04 ± 0.01	3.5 ± 0.2	6045.1 ± 342.9	12
OC	113.6 ± 6.8 [b]	0.05 ± 0.01	3.6 ± 0.3	5312.8 ± 408.8	11

Table 3.4: Three point bending of normal and OVX rat femurs (normalized data).

[b] reflects a significance of $p<0.1$ vs. NC

Torsion Testing

There were no significant differences in either unnormalized or normalized properties of the femur in torsion testing (Table 3.5; 3.6). However, parameters reflect the trends that were seen in three point bending tests, indicating that OVX weakens cortical bone but this weakening is not significant.

Group	Failure Torque (N·mm)	Angular Deformation at Failure (rad)	Energy to Failure (N·mm·rad)	Stiffness (N/mm)	n
NC	395.7 ± 33.2	0.18 ± 0.01	41.7 ± 4.5	2345.3 ± 167.8	15
OC	362.5 ± 26.8	0.21 ± 0.02	42.4 ± 3.3	2007.5 ± 167.8	14

Table 3.5: Torsion testing of normal and OVX rat femurs (unnormalized data).

Group	Shear Stress (MPa)	Shear Strain (%)	Energy to Failure (mJ/mm^3)	Shear Modulus (MPa)	n
NC	73.4 ± 7.6	2.58 ± 0.18	0.31 ± 0.03	3113.7 ± 311.9	15
OC	61.2 ± 4.2	2.90 ± 0.20	0.33 ± 0.03	2478.1 ± 212.0	14

Table 3.6: Torsion testing of normal and OVX rat femurs (normalized data).

3.3.3 Structure: Femoral Cross-Section

OVX caused a significant alteration in the structure of the femur in the mid–diaphysis region. The medial–lateral inner diameter of the OVX controls was significantly ($p<0.05$)

larger than that of the normal controls (Table 3.7). There was also a significantly ($p<0.05$) decreased lateral thickness of the OVX controls compared to the normal controls (Table 3.8).

Group	Medial–Lateral		Posterior–Anterior		n
	Outer Diameter (mm)	Inner Diameter (mm)	Outer Diameter (mm)	Inner Diameter	
NC	3.5 ± 0.1	2.4 ± 0.1	3.2 ± 0.1	2.0 ± 0.1	11
OC	3.6 ± 0.1	2.6 ± 0.1 [a]	2.0 ± 0.1	2.0 ± 0.1	10

Table 3.7: Diameters of normal and OVX rat femurs.

[a]reflects a significance of $p<0.05$ vs. NC

Group	Lateral (mm)	Medial (mm)	Posterior (mm)	Anterior (mm)	n
NC	0.57 ± 0.02	0.58 ± 0.03	0.52 ± 0.02	0.70 ± 0.02	11
OC	0.48 ± 0.02 [a]	0.52 ± 0.03	0.48 ± 0.03	0.64 ± 0.03	10

Table 3.8: Thicknesses of normal and OVX rat femurs.

[a]reflects a significance of $p<0.05$ vs. NC

3.3.4 Mineralization

Mineralization parameters were measured BSE and microhardness. In BSE, the maximum grey level reflects the degree of mineralization, while the maximum intensity refers to the amount of bone that is at that particular grey level. The width at half maximum intensity reflects mineral distribution such that a small width represents a homegeneous

material and a large width reflects a heterogeneous materal. Logit reflects the shape of the distribution curve, thereby encompasing the maximum grey level, intensity and width at half maximum height into one parameter. This parameter is often useful as a means of comparison although its meaning is not intuitively obvious. Microhardness, provides an average hardness, which reflects the average degree of mineralization, from ten chosen test points.

Back Scattered Electron Imaging

There were no significant differences in back scattered electron imaging parameters between OVX and normal controls (Figure 3.3; Table 3.9).

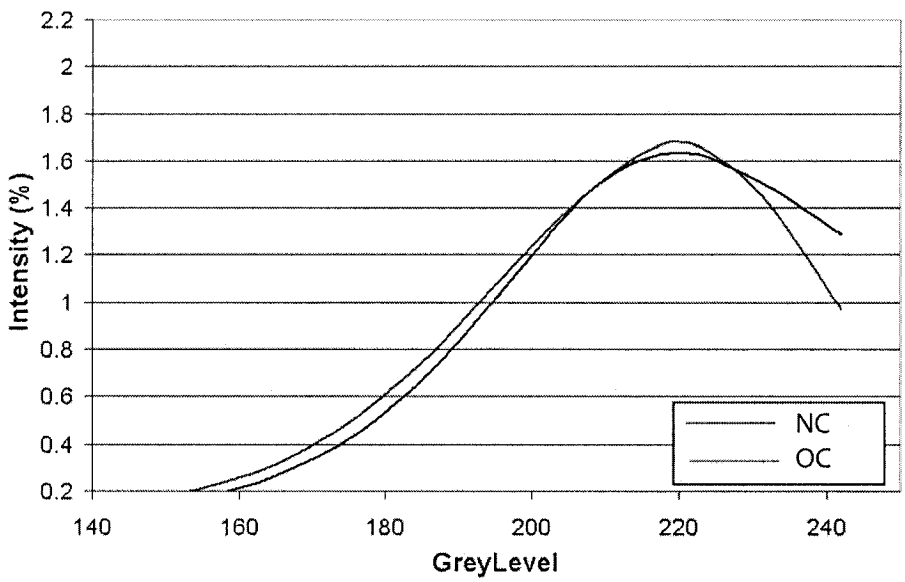

Figure 3.3: BSE distribution curves: comparing cortical bone mineralization in normal and OVX rats

Group	Maximum Grey Level	Maximum Intensity (%)	Width at Half Maximum Intensity	Logit	n
NC	218.8 ± 3.3	2.4 ± 0.1	42.5 ± 2.6	-0.7 ± 0.2	13
OC	224.0 ± 4.1	2.5 ± 0.1	40.9 ± 4.7	-0.8 ± 0.2	12

Table 3.9: BSE imaging of cortical bone in normal and OVX rat tibia.

Microhardness

While there were no significant differences in BSE parameters, there was a decreasing trend ($p<0.1$) in the average hardness of the OVX controls compared to the normal controls, which reflects a decrease in the degree of mineralization due to OVX (Table 3.10).

Group	Average Hardness (H)	n
NC	43.1 ± 0.6	13
OC	41.9 ± 0.4 [b]	14

Table 3.10: Hardness of cortical bone in normal and OVX rat tibia.

[b] reflects a significance of $p<0.1$ vs. NC

3.4 The Effect of OVX on Trabecular Bone

3.4.1 Bone Mineral Density: DXA

The effect of OVX on bone mineral density (BMD) and bone mineral content (BMC) was analyzed using Dual Energy X-Ray Absorptiometry (DXA). In the trabecular bone of the vertebrae (L4+L5+L6), the BMD of the OVX controls was significantly ($p<0.05$) lower than that of the normal controls (Figure 3.4). There was also a decreasing trend ($p<0.1$) in the corresponding BMC values (Table 3.11). This indicates that OVX induced significant trabecular bone loss.

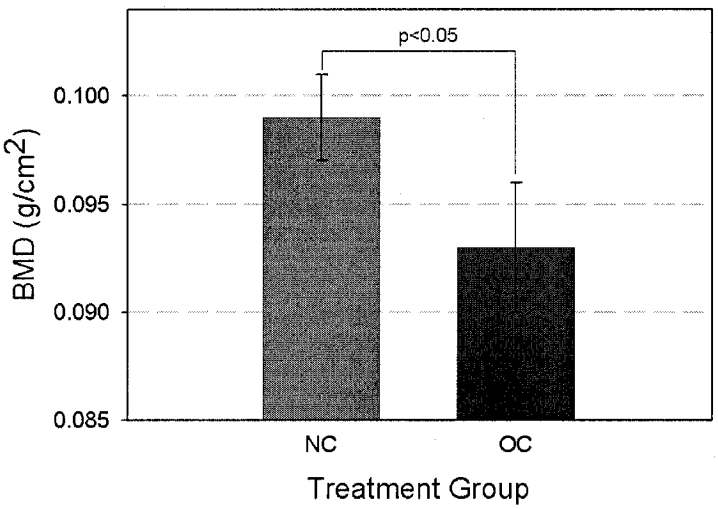

Figure 3.4: Bone Mineral Density (BMD) of the lumber vertebrae: comparing normal and OVX rats.

Group	BMD (g/cm^2)	BMC (g)	n
NC	0.099 ± 0.002	0.149 ± 0.004	11
OC	0.093 ± 0.003 [a]	0.136 ± 0.006 [b]	11

Table 3.11: Vertebral BMD and BMC of normal and OVX rats.

[a]reflects a significance of $p<0.05$ vs. NC [b] reflects a significance of $p<0.1$ vs. NC

3.4.2 Mechanical Properties

Trabecular bone mechanical properties were determined through femoral neck fracture tests and vertebral compression. While femoral neck fracture reflects clinically significant properties, it is a less pure trabecular bone test than vertebral compression due to the mixture of cortical and trabecular bone and complex geometry in the neck region.

Femoral Neck Fracture

Due to the complex geometry of the femoral neck, this data could not be normalized. However, the unnormalized failure load, energy to failure and stiffness of the OVX controls were significantly ($p<0.05$) lower than the normal controls (Table 3.12). This indicates that OVX significantly weakened the trabecular bone in the femoral neck region

Group	Failure Load (N)	Failure Displacement (mm)	Energy to Failure (mJ)	Stiffness (N/mm)	n
NC	176.7 ± 8.2	1.1 ± 0.1	90.7 ± 6.9	335.8 ± 16.2	14
OC	145.1 ± 8.8 [a]	1.2 ± 0.1	71.0 ± 5.7 [a]	218.0 ± 19.8 [a]	11

Table 3.12: Femoral neck fracture of normal and OVX rat femurs.

[a]reflects a significance of $p<0.05$ vs. NC

Vertebral Compression

There was a decreasing trend ($p<0.1$) in the failure load and failure stress of the OVX controls compared to the normal controls. Similarly, the stiffness and elastic modulus of the OVX controls were significantly lower ($p<0.05$) than the normal controls. Conversely, there was an increasing trend ($p<0.1$) in the failure displacement of OVX controls

(Table 3.13; Table 3.14). Overall, these parameters suggest an overall weakening in the trabecular bone of the vertebrae due to OVX.

Group	Failure Load (N)	Failure Displacement (mm)	Energy to Failure (mJ)	Stiffness (N/mm)	n
NC	119.5 ± 3.9	0.41 ± 0.02	26.6 ± 1.7	330.8 ± 13.2	11
OC	107.7 ± 5.8 [b]	0.51 ± 0.06 [b]	29.7 ± 3.4	264.5 ± 37.0 [b]	9

Table 3.13: Vertebral Compression of normal and OVX rat vertebrae (unnormalized data).

[b] reflects a significance of $p<0.1$ vs. NC

Group	Failure Stress (MPa)	Failure Strain (%)	Energy to Failure (MJ/mm^3Pa)	Elastic Modulus (MPa)	n
NC	17.8 ± 1.1	0.26 ± 0.02	2.1 ± 0.2	151.5 ± 9.7	14
OC	15.2 ± 1.1 [b]	0.27 ± 0.03	1.8 ± 0.2	98.6 ± ?	11

Table 3.14: Vertebral Compression of normal and OVX rat vertebrae (normalized data).

[b] reflects a significance of $p<0.1$ vs. NC

3.4.3 Trabecular and Connectivity Analysis

The OVX controls had significantly ($p<0.05$) lower trabecular bone volume along with significantly ($p<0.05$) lower trabecular thickness and number. This implies that the OVX significantly deteriorated trabecular structure (Table 3.15). This correlates with

the connectivity data in which the OVX controls had a significantly ($p<0.05$) lower total skeleton length. Furthermore, OVX controls had less connected trabeculae as shown by the significantly lower number of multiple points and length of node–node struts ($p<0.05$; Table 3.16).

Group	Trabecular Bone Volume (%)	Average Trabecular Thickness (μm)	Trabecular Number	Trabecular Separation (μm)	n
NC	18.4 ± 1.8	71.4 ± 2.7	2.6 ± 0.2	358.3 ± 50.1	11
OC	12.3 ± 1.1 [a]	61.9 ± 2.1 [a]	2.0 ± 0.2 [a]	507.0 ± 71.7	13

Table 3.15: Trabecular structure of the proximal tibia in normal and OVX rats.
[a]reflects a significance of $p<0.05$ vs. NC

Group	Total Skeleton Length (mm/mm^2)	Node–Node Strut Length (mm/mm^2)	Node–Free Strut Length (mm/mm^2)	Free–Free Strut Length (mm/mm^2)	Number of Multiple Points ($\#/mm^2$)	n
NC	2.5 ± 0.3	0.9 ± 0.2	0.8 ± 0.1	0.3 ± 0.1	4.6 ± 0.8	11
OC	1.8 ± 0.2 [a]	0.2 ± 0.1 [a]	0.6 ± 0.1	0.3 ± 0.1	2.4 ± 0.3 [a]	13

Table 3.16: Trabecular connectivity of the proximal tibia in normal and OVX rats.
[a]reflects a significance of $p<0.05$ vs. NC

3.4.4 Trabecular Remodeling: Histomorphometry

Remodeling parameters were measured with static histomorphometry although the eroded surface was not measured as a result of and therefore only formation parameters are reported. Analysis of the osteoid showed a significantly ($p<0.05$) higher osteoid surface in the OVX controls than in the normal controls. Similarly, the osteoid volume was higher in the OVX controls although not to significance (Table 3.17). Overall, this shows an increase in bone formation due to OVX.

Group	Osteoid Volume (%)	Osteoid Surface (%)	Osteoid Volume/ Bone Volume(%)	n
NC	0.5 ± 0.1	7.7 ± 1.7	4.0 ± 1.1	13
OC	0.8 ± 0.1	16.4 ± 2.3 [a]	6.0 ± 1.0	11

Table 3.17: Histomorphometry parameters of normal and OVX rats.
[a]reflects a significance of $p<0.05$ vs. NC

3.4.5 Mineralization

Mineralization parameters were reflected with back scattered electron imaging (BSE) and microhardness. In BSE, the maximum grey level reflects the degree of mineralization, while the maximum intensity refers to the amount of bone that is at that grey level. The width at half maximum intensity indicates mineral distribution and logit reflects the shape of the distribution curve. Microhardness provides an average hardness, which reflects the average degree of mineralization, test points chosen on ten separate trabeculae.

Back Scattered Electron Imaging

The maximum grey level of the OVX controls was significantly ($p<0.05$) lower than that of the normal controls. This reflects a decrease in mineralization level due to OVX (Table 3.18). Meanwhile, the logit function of the OVX controls was significantly ($p<0.05$) higher than that of the normal controls and this was reflected in the shape of the distribution as shown in Figure 3.5 in which the left shift in grey level is the most prominent feature.

Group	Maximum Grey Level	Maximum Intensity (%)	Width at Half Maximum Intensity	Logit	n
NC	190.1 ± 3.1	1.6 ± 0.1	59.9 ± 2.6	0.8 ± 0.1	13
OC	178.0 ± 1.9[a]	1.6 ± 0.1	59.3 ± 4.4	1.3 ± 0.1 [a]	11

Table 3.18: BSE imaging of the trabecular bone in normal and OVX rat tibia.

[a]reflects a significance of $p<0.05$ vs. NC

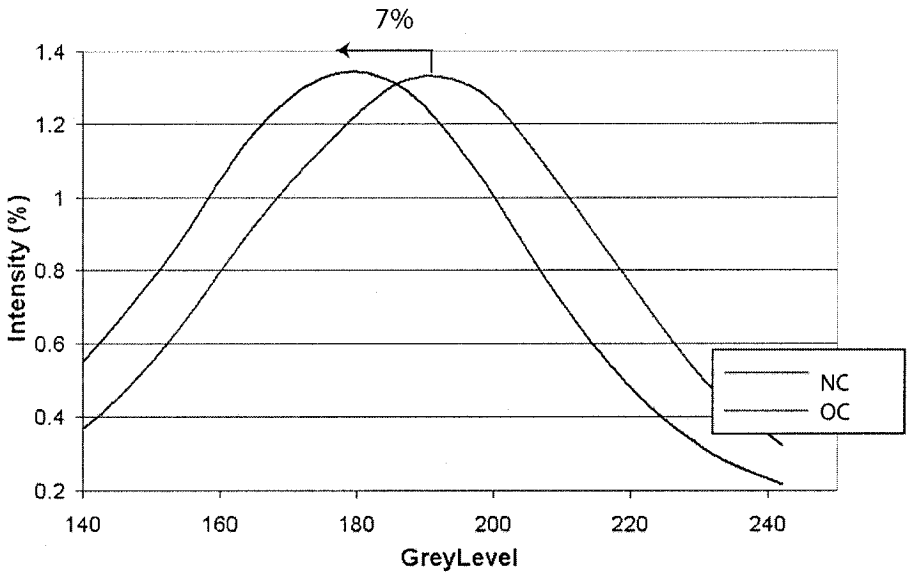

Figure 3.5: Mineral distribution curves from Back Scattered Electron Imaging: comparing the mineralization of trabecular bone in normal and OVX rats

Microhardness

While OVX was shown to cause a decrease in mineralization when analyzed with BSE, microhardness tests did not show any significant differences (Table 3.19).

Group	Average Hardness (H)	n
NC	39.3 ± 0.5	13
OC	38.7 ± 0.5	14

Table 3.19: Hardness of trabecular bone in OVX and normal rat tibia.

3.5 Summary and Discussion of Results

Along with causing a 20% increase in weight gain, OVX significantly compromised bone quality and increased bone fragility. The increased fragility was shown through decreased failure strength, energy to failure and stiffness. Fragility is dependent on the underlying bone quality. In the OVX skeleton there was a decrease in both cortical and trabecular BMD which reflects a decrease in overall bone mass. Structurally, in cortical bone, OVX increased the inner diameter of the femur and decreased bone thickness. Meanwhile, in trabecular bone, OVX decreased the quantity and quality of trabeculae and also reduced connectivity. Furthermore, OVX increased bone formation as reflected in the increased osteoid surface. This increased trabecular bone formation in combination with a deteriorated trabecular structure implies that there was an increased bone turnover due to OVX and that there was an imbalance between resorption and formation . Additionally, there was a decrease in mineralization, which was especially evident in the trabecular bone although this was also evidenced in terms of a decrease in the hardness of the cortical bone. Overall, while OVX affected both cortical and trabecular bone, the trabecular effects were more prominent.

Chapter 4

Results: The Skeletal Effects of AOD

4.1 Introduction

This chapter will investigate the effect of AOD treatment on the normal rat skeleton as a control to treatment on the OVX skeleton. This was accomplished through daily oral treatments for a period of 12 weeks. For the sake of clarity as well as consistency with the other results chapters, this chapter is divided into the effect of AOD on body weight, cortical bone and trabecular bone. All data is expressed as mean $\pm$ standard error of mean (SEM) and ^{a} reflects a significance of $p<0.05$ vs. normal control while ^{b} reflects a significance of $p<0.1$ vs. normal control.

4.2 The Effect of AOD on Body Weight

AOD had very little effect on the weight of the normal model. Neither AOD–0.25 nor AOD–0.5 produced a significant change; however, there was a slight although not statistically significant decrease with AOD–0.5 (Figure 4.1, Table 4.1).

Group	Initial Weight (g)	Final Weight (g)	Weight Gained (%)	n
NC	339.1 ± 8.3	343.9 ± 11.0	1.4 ± 2	13
N(0.25)	320.2 ± 3.4	321.0 ± 5.0	0.4 ± 1.1	15
N(0.5)	324.1 ± 3.1	315.7 ± 5.3	-2.6 ± 1.1	15

Table 4.1: Body weight of AOD treated rats.

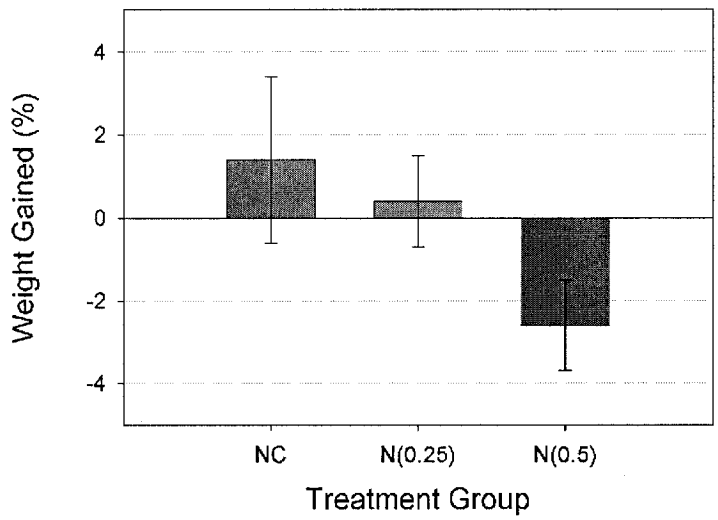

Figure 4.1: Percentage of body weight change: comparing N(0.25), N(0.5) and NC groups

4.3 The Effect of AOD on Cortical Bone

4.3.1 Bone Mineral Density: DXA

The effect of AOD on bone mineral density (BMD) and bone mineral content (BMC) was analyzed using Dual Energy X–Ray Absorptiometry (DXA). In the cortical bone of the left femur AOD–0.25 had no effect; however, AOD–0.5 caused a significant ($p<0.05$) increase in femoral BMD over the normal controls (Figure 4.2, Table 4.2). This indicates that AOD–0.5 may induce an increase in bone and that this increase may be dose–dependent.

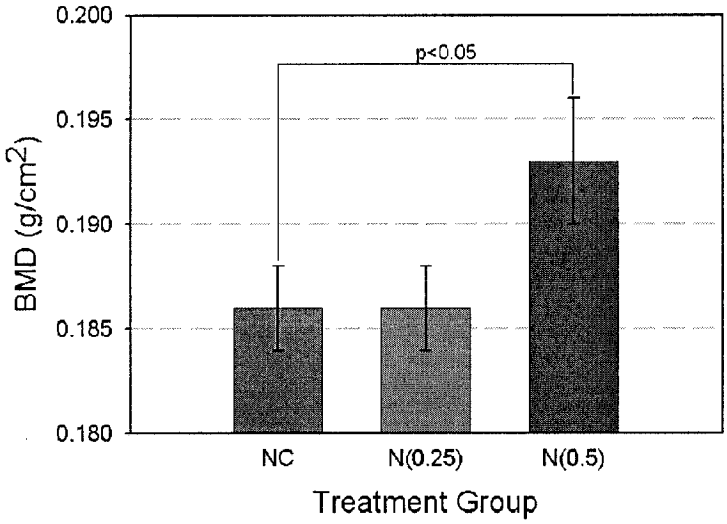

Figure 4.2: BMD of the left femur: comparing N(0.25), N(0.5) and NC groups.

Group	BMD (g/cm^2)	BMC (g)	n
NC	0.186 ± 0.002	0.503 ± 0.009	15
N(0.25)	0.186 ± 0.002	0.499 ± 0.011	14
N(0.5)	0.193 ± 0.003 [a]	0.525 ± 0.013	15

Table 4.2: Femoral BMD and BMC of AOD treated rats.

[a]reflects a significance of $p<0.05$ vs. NC

4.3.2 Mechanical Properties

Cortical bone mechanical properties were determined through three point bending and torsion tests. The right and left femurs were used respectively.

Three–point bending

Although there were no significant changes in the unnormalized or normalized properties, there was an increasing trend ($p<0.1$) in the failure load of AOD–0.5 compared to the normal controls (Table 4.3). This increase was also reflected in the failure stress as well as

the stiffness and elastic modulus although not to significance (Table 4.4). Nevertheless, these trends may indicate an increased cortical strength due to AOD–0.5 treatment. However, such an increase was not apparent with AOD–0.25 treatment.

Group	Failure Load (N)	Failure Displacement (mm)	Energy to Failure (mJ)	Stiffness (N/mm)	n
NC	159.4 ± 4.8	0.55 ± 0.02	57.0 ± 4.1	566.1 ± 21.9	14
N(0.25)	155.7 ± 6.2	0.58 ± 0.03	59.2 ± 3.5	553.1 ± 29.2	14
N(0.5)	173.4 ± 6.0 [b]	0.53 ± 0.02	57.0 ± 3.0	614.2 ± 19.9	14

Table 4.3: Three point bending of AOD treated rat femurs (unnormalized data).

[b] reflects a significance of $p<0.1$ vs. NC

Group	Failure Stress (MPa)	Failure Strain (mm/mm)	Energy to Failure (MPa)	Elastic Modulus (MPa)	n
NC	130.6 ± 5.2	0.04 ± 0.01	3.5 ± 0.2	6045.1 ± 342.9	12
N(0.25)	123.4 ± 8.0	0.05 ± 0.01	3.8 ± 0.3	5940.0 ± 476.1	11
N(0.5)	141.2 ± 5.7	0.04 ± 0.01	3.6 ± 0.2	6461.6 ± 369.8	13

Table 4.4: Three point bending of AOD treated rat femurs (normalized data).

Torsion Testing

Cortical changes were more apparent in torsion testing than they were in three point bending tests. While there were no significant differences in failure torque and failure shear stress with either AOD dose, there was an increasing trend ($p<0.1$) in the stiffness and shear modulus of AOD–0.5 compared to normal controls. There was also an increasing trend ($p<0.1$) in unnormalized energy to failure of AOD–0.5 over normal controls. The combination of these trends may indicate an increased strength due to AOD–0.5 treatment.

Comparatively, AOD–0.25 had a significantly ($p<0.05$) higher unnormalized energy to failure than the normal controls. Furthermore, the angular deformation at failure and the shear strain of the AOD–0.25 group were significantly ($p<0.05$) higher than the normal controls. These results indicate that AOD–0.25 improved the toughness of cortical bone. These results are shown in Table 4.5 and Table 4.6

Group	Failure Torque (N·mm)	Angular Deformation at Failure (rad)	Energy to Failure (N·mm·rad)	Stiffness (N/mm)	n
NC	395.7 ± 33.2	0.18 ± 0.01	41.7 ± 4.5	2345.3 ± 167.8	15
N(0.25)	393.5 ± 30.2	0.27 ± 0.02 [a]	59.0 ± 5.2 [a]	1865.5 ± 195.6	10
N(0.5)	424.4 ± 31.9	0.22 ± 0.02 [b]	54.7 ± 5.9 [b]	2231.3 ± 237.2	12

Table 4.5: Torsion testing of AOD treated rat femurs (unnormalized data).
[a]reflects a significance of $p<0.05$vs. NC; [b] reflects a significance of $p<0.1$ vs. NC

Group	Shear Stress (MPa)	Shear Strain (%)	Energy to Failure (mJ/mm^3)	Shear Modulus (MPa)	n
NC	73.4 ± 7.6	2.6 ± 0.2	0.31 ± 0.03	3113.7 ± 311.9	15
N(0.25)	65.2 ± 4.8	3.6± 0.2 [a]	0.42 ± 0.04 [b]	2324.0 ± 240.3 [b]	10
N(0.5)	72.6 ± 4.5	2.9 ± 0.3	0.39 ± 0.04	2933.3 ± 320.6	13

Table 4.6: Torsion testing of AOD treated rat femurs (normalized data).

[a]reflects a significance of $p<0.05$ vs. NC; [b] reflects a significance of $p<0.1$ vs. NC

4.3.3 Structure: Femoral Cross-Section

AOD altered the amount and distribution of bone in the femur. This was evidenced by an increasing trend ($p<0.1$) in the medial-lateral outer diameter of the N(0.5) group compared to normal controls (Table 4.7). AOD–0.25, on the other hand, caused an increasing trend in the anterior-posterior inner diameter ($p<0.1$). AOD–0.25 also increased outer diameters although these values were not significant (Table 4.7).

Group	Medial–Lateral		Posterior–Anterior		n
	Outer Diameter (mm)	Inner Diameter (mm)	Outer Diameter (mm)	Inner Diameter	
NC	3.53 ± 0.07	2.38 ± 0.04	3.18 ± 0.05	1.97 ± 0.05	11
N(0.25)	3.55 ± 0.03	2.45 ± 0.05	3.26 ± 0.04	2.12 ± 0.06 [b]	11
N(0.5)	3.68 ± 0.07 [b]	2.48 ± 0.09	3.16 ± 0.07	1.97 ± 0.06	13

Table 4.7: Diameters of AOD treated rat femurs.

[b] reflects a significance of $p<0.1$ vs. NC

Group	Lateral Thickness(mm)	Medial Thickness(mm)	Posterior Thickness(mm)	Anterior Thickness(mm)	n
NC	0.57 ± 0.02	0.58 ± 0.03	0.52 ± 0.02	0.70 ± 0.02	11
N(0.25)	0.53± 0.02	0.56 ± 0.02	0.48 ± 0.03	0.66 ± 0.02	11
N(0.5)	0.57 ± 0.04	0.62 ± 0.04	0.54 ± 0.02	0.65 ± 0.03	13

Table 4.8: Thicknesses of AOD treated rat femurs.

4.3.4 Mineralization

Mineralization parameters were reflected with BSE and microhardness as discussed in section 3.3.4.

Back Scattered Electron Imaging

AOD–0.25 significantly ($p<0.05$) increased both the maximum grey level and intensity (Table 4.9). This reflects a significant increase in both the degree of mineralization and also the amount of bone present at that increased level. This was also reflected by the increasing trend ($p<0.1$) in the logit function, which indicates an alteration in the mineral distribution (Figure 4.3).

While a significant change in mineralization was not apparent with AOD–0.5, this dose caused an increasing trend ($p<0.1$) in the maximum intensity compared to the normal controls, which is reflected in the higher peak height of the curve (Figure 4.3). This indicates that there may be an abundance of a particular mineral level but this level does not have a significantly higher degree of mineralization than the normal controls.

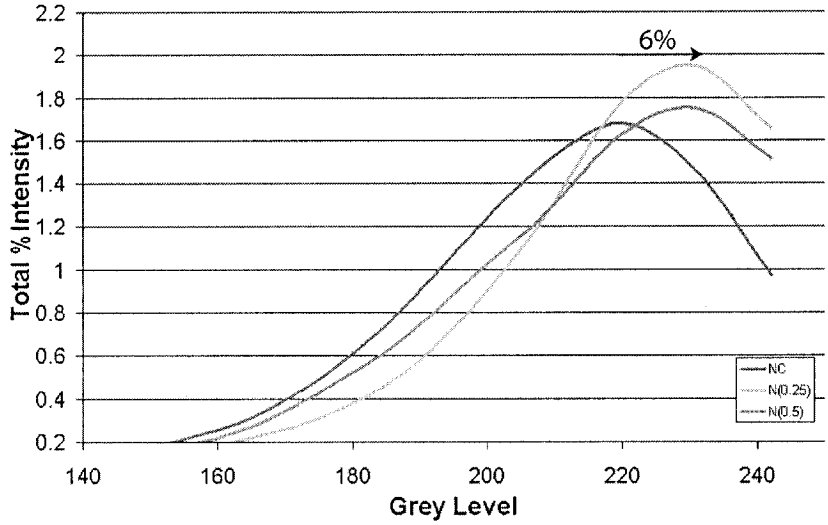

Figure 4.3: BSE distribution curves: comparing cortical bone mineralization in N(0.25), N(0.5) and NC groups

Group	Maximum Grey Level	Maximum Intensity (%)	Width at Half Maximum Intensity	Logit	n
NC	218.8 ± 3.3	2.4 ± 0.1	42.5 ± 2.6	-0.7 ± 0.2	13
N(0.25)	232.1 ± 2.5 [a]	2.7 ± 0.1 [a]	41.6 ± 1.5	-1.2 ± 0.1 [b]	15
N(0.5)	225.4 ± 4.2	2.6 ± 0.1 [b]	39.2 ± 1.9	-1.0 ± 0.2	14

Table 4.9: BSE imaging of the cortical bone in AOD treated rat tibia.
[a]reflects a significance of $p<0.05$ vs. NC; [b] reflects a significance of $p<0.1$ vs. NC

Microhardness

Although differences in mineralization were apparent from BSE analysis, such differences were not observed in microhardness testing. These tests revealed no significant differences

in the hardness of the AOD dosed groups compared to the normal controls (Table 4.10).

Group	Average Hardness (H)	n
NC	43.1 ± 0.6	13
N(0.25)	42.6 ± 0.4	15
N(0.5)	43.0 ± 0.4	14

Table 4.10: Hardness of cortical bone in AOD treated rat tibia.

4.4 The Effect of AOD on Trabecular Bone

4.4.1 Bone Mineral Density: DXA

The effect of AOD on bone mineral density (BMD) and bone mineral content (BMC) was analyzed using Dual Energy X–Ray Absorptiometry (DXA). In the trabecular bone of the vertebrae (L4+L5+L6), neither dose of AOD appeared to have significant effects, which indicates that AOD did not affect bone quantity in trabecular bone (Figure, 4.4; Table 4.11).

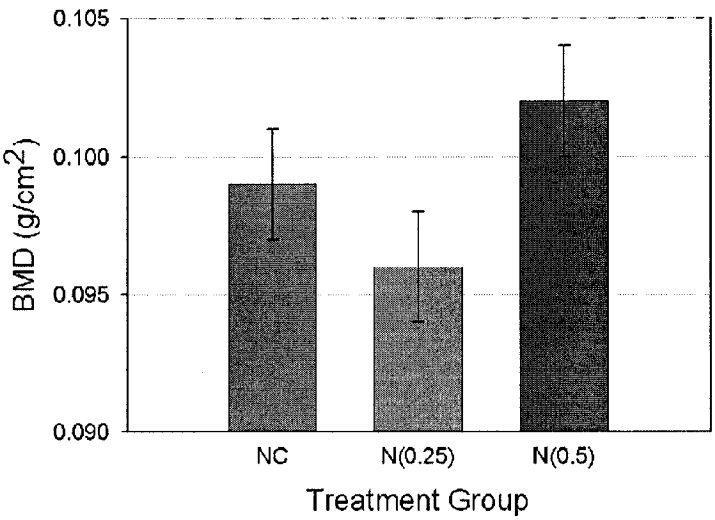

Figure 4.4: Bone Mineral Density (BMD) of the lumber vertebrae: comparing N(0.25), N(0.5) and normal control rats.

Group	BMD (g/cm^2)	BMC (g)	n
NC	0.099 ± 0.002	0.149 ± 0.004	11
N(0.25)	0.096 ± 0.002	0.143 ± 0.003	11
N(0.5)	0.102 ± 0.002	0.154 ± 0.005	12

Table 4.11: Vertebral BMD and BMC of AOD treated rats.

4.4.2 Mechanical Properties

Trabecular bone mechanical properties were determined through femoral neck fracture tests and vertebrae compression. While femoral neck fracture reflects clinically significant properties, it is a less pure trabecular bone test than vertebrae compression due to the mixture of cortical and trabecular bone and the complex geometry in the neck region.

Femoral Neck Fracture

Due to the complex geometry of the femoral neck, this data could not be normalized. However, unnormalized data showed that AOD–0.5 increased the failure load over that of the normal controls although not to significance.

AOD–0.25, on the other hand, significantly ($p<0.05$) increased the failure displacement and caused an increasing trend ($p<0.1$) in energy to failure. Additionally, there was a decreasing trend ($p<0.1$) in the stiffness of AOD–0.25 compared to normal controls (Table 4.12). These results indicate that AOD–0.25 improves the toughness of the trabecular bone in the femoral neck region.

Group	Failure Load (N)	Failure Displacement (mm)	Energy to Failure (mJ)	Stiffness (N/mm)	n
NC	176.7 ± 8.2	1.1 ± 0.1	90.7 ± 6.9	335.8 ± 16.2	14
N(0.25)	118.2 ± 3.8	0.50 ± 0.04 [a]	31.4 ± 2.3 [b]	280.0 ± 26.1 [b]	10
N(0.5)	127.9 ± 4.0	0.40 ± 0.03	26.7 ± 1.9	350.7 ± 23.2	9

Table 4.12: Femoral neck fracture of AOD treated rat femurs.

[a]reflects a significance of $p<0.05$ vs. NC; [b] reflects a significance of $p<0.1$ vs. NC

Vertebral Compression

There were no significant effects of AOD on the mechanical properties of the vertebrae. However, there appeared to be a slight increase in failure load with AOD–0.25 and a slight decrease in elastic modulus with AOD–0.5 compared to normal controls (Table 4.13; Table 4.14).

Group	Failure Load (N)	Failure Displacement (mm)	Energy to Failure (mJ)	Stiffness (N/mm)	n
NC	119.4 ± 3.9	0.41 ± 0.02	26.6 ± 1.7	330.8 ± 13.2	11
N(0.25)	192.0 ± 16.8	1.3 ±0.1	97.0 ± 10.2	313.8 ± 34.6	14
N(0.5)	189.3 ± 19.6	1.1 ±0.1	89.1 ± 9.4	303.6 ± 38.7	10

Table 4.13: Vertebral compression of AOD treated rat vertebrae (unnormalized data).

Group	Failure Stress (MPa)	Failure Strain (%)	Energy to Failure (MJ/mm^3Pa)	Elastic Modulus (MPa)	n
NC	17.8 ± 1.1	0.26 ± 0.02	2.1 ± 0.2	151.5 ± 9.7	14
N(0.25)	19.9 ± 1.4	0.30 ± 0.02	2.3 ± 0.2	142.3 ± 11.1	14
N(0.5)	18.7 ± 1.9	0.25 ±0.02	2.1 ±0.2	124.5 ± 15.0	10

Table 4.14: Vertebral compression of AOD treated rat vertebrae (normalized data).

4.4.3 Trabecular Structure and Connectivity Analysis

There were no significant differences in the structural parameters between the N(0.25), N(0.5) and the normal controls as shown in Table 4.15. However, there was an increasing trend ($p<0.1$) in the length of node-free struts of N(0.5) (Table 4.16) although this solitary value provides little indication of any significant changes.

Group	Trabecular Bone Volume (%)	Average Trabecular Thickness(μm)	Trabecular Number	Trabecular Separation (μm)	n
NC	18.4 ± 1.8	71.4 ± 2.7	2.6 ± 0.2	358.3 ± 50.1	11
N(0.25)	17.5 ± 2.6	67.4 ± 3.5	2.5 ± 0.3	423.9 ± 83.6	14
N(0.5)	20.2 ± 2.4	65.8 ± 2.9	3.0 ± 0.3	289.5 ± 32.4	10

Table 4.15: Trabecular structure of AOD treated rats proximal tibia.

Group	Length of Total Skeleton (mm/mm^2)	Length of Node–Node Struts (mm/mm^2)	Length of Node–Free Struts (mm/mm^2)	Length of Free–Free Struts (mm/mm^2)	Number of Multiple Points (#/mm^2)	n
NC	2.50 ± 0.26	0.86 ± 0.17	0.75 ± 0.11	0.34 ± 0.04	4.56 ± 0.77	11
N(0.25)	2.38 ± 0.29	0.74 ± 0.20	0.72 ± 0.10	0.35± 0.07	4.31 ± 0.76	12
N(0.5)	2.94 ± 0.29	0.90 ± 0.19	1.01 ± 0.09 [b]	0.31 ± 0.05	5.15 ± 0.84	10

Table 4.16: Trabecular connectivity AOD treated rats proximal tibia.

[b] reflects a significance of $p<0.1$ vs. NC

4.4.4 Trabecular Remodeling: Histomorphometry

Remodeling parameters were measured with static histomorphometry. AOD–0.25 caused an increasing trend ($p<0.1$) in the osteoid surface compared to normal controls, which may reflect an increased bone formation (Table 4.17). Contrarily, AOD–0.5 had no significant bone formation effects.

Group	Osteoid Volume (%)	Osteoid Surface (%)	Osteoid Volume/ Bone Volume (%)	n
NC	0.5 ± 0.1	7.7 ± 1.7	4.0 ± 1.1	13
N(0.25)	0.5 ± 0.1	12.6 ± 1.9 [b]	4.2 ± 0.6	12
N(0.5)	0.4 ± 0.1	9.7 ± 1.7	2.9 ± 1.1	13

Table 4.17: Histomorphometry parameters of AOD treated rats.

[b] reflects a significance of $p<0.1$ vs. NC

4.4.5 Mineralization

Back Scattered Electron Imaging

There were no significant differences in BSE parameters between N(0.25) and the normal controls, which indicates that AOD–0.25 did not significantly affect trabecular mineralization. Contrarily, effects were observed with AOD–0.5. The width at half maximum intensity of N(0.5) was significantly ($p<0.05$) lower than that of the normal controls, which reflects a decrease in the heterogeneity of the mineral distribution. This was accompanied by an increasing trend ($p<0.1$) in maximum intensity indicating an increased amount of mineral at a particular mineralization level (Table 4.18).

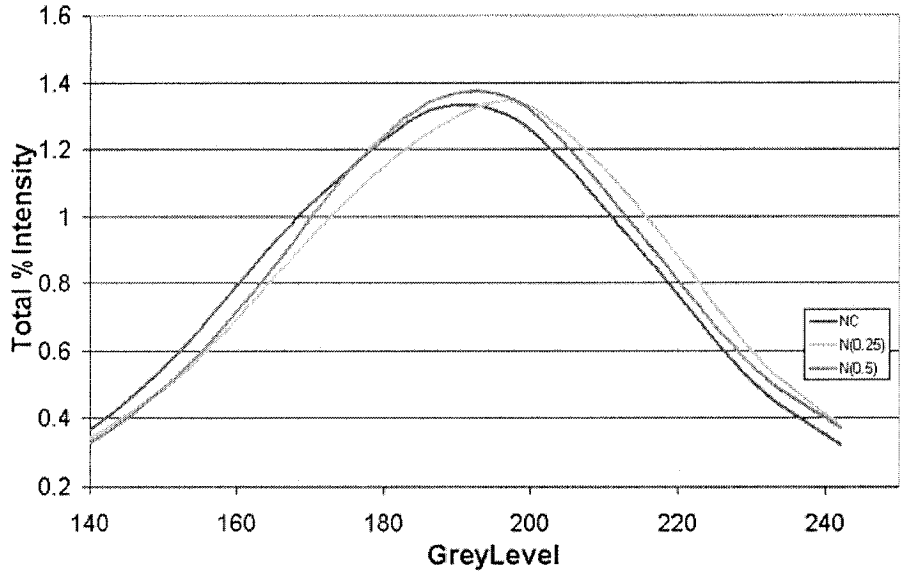

Figure 4.5: BSE distribution curves: comparing trabecular bone mineralization in N(0.25), N(0.5) and NC groups

Group	Maximum Grey Level	Maximum Intensity (%)	Width at Half Maximum Intensity	Logit	n
NC	190.1 ± 3.1	1.59 ± 0.05	59.9 ± 2.6	0.8 ± 0.1	13
N(0.25)	195.3 ± 3.4	1.66 ± 0.05	55.8 ± 2.5	0.6 ± 0.2	13
N(0.5)	192.3 ± 2.9	1.72 ± 0.05 [b]	52.1 ± 2.7 [a]	0.7 ± 0.2	14

Table 4.18: BSE imaging of the trabecular bone in AOD treated rat tibia.

[a]reflects a significance of $p<0.05$ vs. NC; [b] reflects a significance of $p<0.1$ vs. NC

4.4.6 Microhardness

Similar to BSE, microhardness tests showed no differences in the degree of mineralization due to AOD treatment (Table 4.19). Since microhardness probes one small area it does not have the capacity to judge mineral distribution and therefore we would not expect to see changes in heterogeneity as we saw with the BSE testing (Table 4.19).

Group	Average Hardness (H)	n
NC	39.3 ± 0.5	13
N(0.25)	39.8 ± 0.5	15
N(0.5)	38.5 ± 0.4	14

Table 4.19: Hardness of trabecular bone in the tibia of AOD treated rats.

4.5 Summary and Discussion of Results

AOD did not cause significant weight changes in the normal model; however, AOD did influence the skeleton. Generally, cortical bone was affected more than trabecular bone and this was true in the case of both doses. Furthermore, there were very few differences in vertebral compression, which opens the possibility that femoral neck effects were actually due to the cortical bone at the site rather than the trabecular bone. The specific effects appeared to be dose–dependent.

AOD–0.25 increased both cortical toughness and trabecular toughness in femoral neck fracture tests as evidenced by increased failure deformation/strain and energy to failure along with decreased stiffness. Although there were no significant differences in load or stress, these values tended to be the same or slightly higher than those of the normal controls, which indicates an increased overall bone strength. This strength increase was accompanied by increased mineralization in cortical bone and bone deposition further

from the central axis. While it appears contradictory to have a decreased stiffness and increased mineralization this may be due to changes in porosity or mineral orientation. In trabecular bone, neither mineralization nor structure were significantly different between N(0.25) and NC but there was an increase in bone formation as reflected by the higher osteoid surface.

AOD–0.5 appeared to improve the strength of cortical bone as reflected by the increased failure load, stiffness/shear modulus and energy to failure although these increases were statistically described as trends rather than significance. This apparent strength increase was associated with a higher BMD and a larger medial-lateral outer diameter, which indicates that bone redistributed further from the central bone axis may be responsible for the strength increase. Nevertheless, differences were not evident in the trabecular bone with AOD–0.5 treatment, except for more homogeneous mineral distribution, which indicates that this dose may not significantly effect trabecular bone.

Chapter 5

Results: The Skeletal Effects of AOD and OVX

5.1 Introduction

This chapter presents the effects of AOD on the ovariectomized rat skeleton. In chapter 3 we saw significant body weight increases along with compromised bone quality and an increased fragility in the OVX skeleton. In chapter 4 we saw that AOD had no weight effects and minimal, although variable, effects in the skeleton. Effects on cortical bone were most significant and dose-dependent. In this chapter we are concerned with the combination of AOD and OVX in an attempt to understand if AOD can prevent the OVX induced bone loss. Combined treatment will be compared to OVX controls and in the case of improvements will also be compared to normal controls. All data is expressed as mean $\pm$ standard error of mean (SEM) and ^{a} reflects a significance of $p<0.05$ vs. OC while ^{b} reflects a significance of $p<0.1$ vs. OC. Meanwhile, ^{c} reflects a significance of $p<0.05$ vs. NC while ^{d} reflects a significance of $p<0.1$ vs. NC.

5.2 The Effect of AOD and OVX on Body Weight

AOD decreased the OVX–induced weight gain by 50%. This effect was significant ($p<0.05$) for both AOD–0.25 and AOD–0.5 (Figure 5.1). However, weight gain was not returned to normal control levels (Table 5.1).

Group	Initial Weight (g)	Final Weight (g)	Weight Gained (%)	n
NC	339.1 ± 8.3	343.9 ± 11.0	1.4 ± 2.0	13
OC	316.9 ± 7.3	382.3 ± 5.4	21.2 ± 2.3	15
O(0.25)	323.4 ± 2.6	357.0 ± 5.3	10.4 ±1.6 [a]	15
O(0.5)	322.8 ± 2.7	361.7 ± 5.1	12.1 ± 1.7 [a]	15

Table 5.1: Body weight of AOD treated OVX rats.

[a] reflects a significance of $p<0.05$ vs. OC

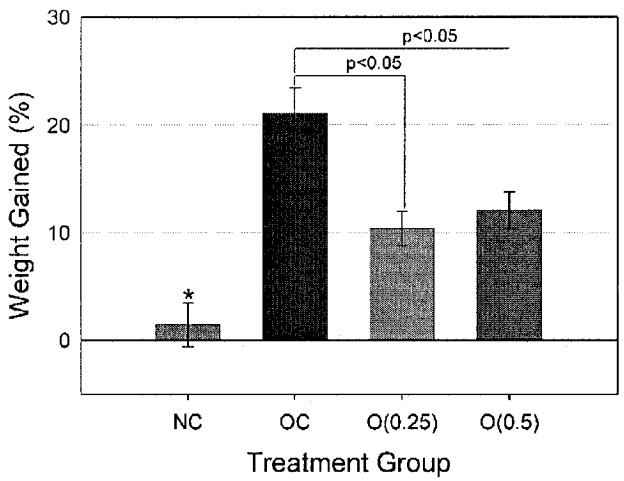

Figure 5.1: Percentage of body weight change: comparing O(0.25) and O(0.5) to normal and OVX control rats.

* reflects a significance of $p<0.05$ vs. all groups

5.3 The Effect of AOD and OVX on Cortical Bone

5.3.1 Bone Mineral Density: DXA

The effect of OVX on bone mineral density (BMD) and bone mineral content (BMC) was analyzed using Dual Energy X–Ray Absorptiometry (DXA). In the cortical bone of the left femur, both O(0.25) and O(0.5) had a slightly higher BMD than the OVX controls (Figure 5.2). The BMD values approached those of the normal controls (Table 5.2). Although this increase was not to significance, this was likely due to the high variability.

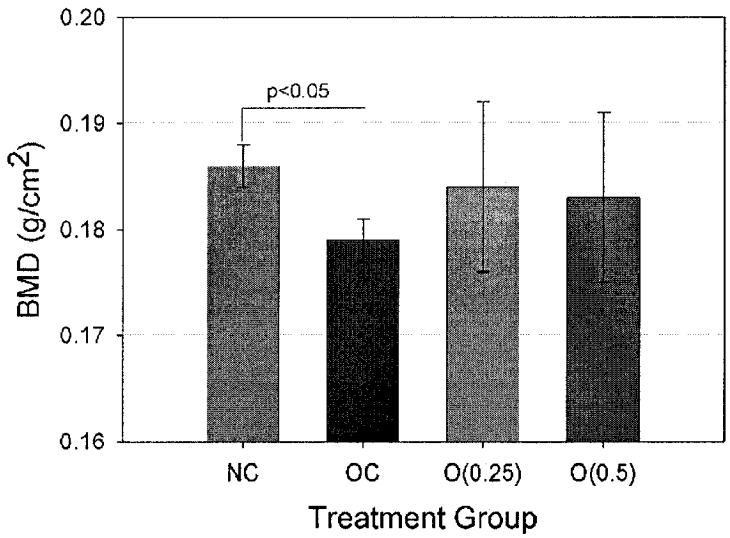

Figure 5.2: Bone Mineral Density (BMD) of the left femur: comparing O(0.25) and O(0.5) to normal and OVX control rats.

Group	BMD (g/cm^2)	BMC (g)	n
NC	0.186 ± 0.002	0.503 ± 0.009	15
OC	0.179 ± 0.002	0.495 ± 0.009	14
O(0.25)	0.184 ± 0.008	0.506 ± 0.009	14
O(0.5)	0.183 ± 0.008	0.502 ± 0.009	14

Table 5.2: Femoral BMD and BMC of AOD treated OVX rats.

5.3.2 Mechanical Properties

Cortical bone mechanical properties were determined through three point bending and torsion tests. The right and left femurs were used respectively.

Three–point bending

Both O(0.25) and O(0.5) groups had significantly ($p<0.05$) higher failure loads than the OVX controls (Table 5.3). In the remaining parameters, however, there were more significant effects with the O(0.5) than the O(0.25) group. There was an increasing trend ($p<0.1$) in the failure stress of O(0.5) compared to OVX controls and the stiffness was also significantly ($p<0.05$) higher (Table 5.4 and 5.3). Contrarily, the failure displacement of O(0.5) was significantly ($p<0.05$) lower than that of the OVX controls. These results indicate an increased strength with both AOD doses.

Group	Failure Load (N)	Failure Displacement (mm)	Energy to Failure (mJ)	Stiffness (N/mm)	n
NC	159.4 ± 4.8	0.55 ± 0.02	57.0 ± 4.1	566.1 ± 21.9	14
OC	146.6 ± 6.8	0.6 ± 0.04	60.6 ± 4.5	522.3 ± 22.8	13
O(0.25)	163.4 ± 4.6 [a]	0.57 ± 0.02	58.7 ± 3.1	561.7 ± 16.2	15
O(0.5)	163.6 ± 6.0 [a]	0.53 ± 0.02 [a]	56.5 ± 4.0	583.6 ± 21.2 [a]	14

Table 5.3: Three point bending of AOD treated OVX rat femurs (unnormalized data). [a] reflects a significance of $p<0.05$ vs. OC

Group	Failure Stress (MPa)	Failure Strain (mm/mm)	Energy to Failure (MPa)	Elastic Modulus (MPa)	n
NC	130.6 ± 5.2	0.04 ± 0.01	3.5 ± 0.2	6045.1 ± 342.9	12
OC	113.6 ± 6.8	0.05 ± 0.01	3.6 ± 0.3	5312.8 ± 408.8	11
O(0.25)	125.7 ± 5.8	0.05 ± 0.01	3.5 ± 0.1	5262.3 ± 444.1	15
O(0.5)	131.6 ± 7.1 [b]	0.04 ± 0.01	3.5 ± 0.2	6026.1 ± 457.7	14

Table 5.4: Three point bending of AOD treated OVX rat femurs (normalized data).

[b] reflects a significance of $p<0.1$ vs. OC

Torsion Testing

In the unnormalized parameters, the failure torque and energy to failure of both O(0.25) and O(0.5) groups were significantly ($p<0.05$) higher than the OVX controls (Table 5.5). The O(0.5) group also had a significantly higher stiffness ($p<0.05$). The normalized effects were more varied. AOD–0.25 caused an increasing trend ($p<0.1$) in the shear strain along with non-significant increases in shear stress and energy to failure (Table 5.6). Meanwhile, AOD–0.5 significantly ($p<0.05$) increased the shear stress and energy to failure, which indicates the strength gain as seen in the unnormalized properties. Overall, these results indicate an increased strength with AOD treatment over OVX controls.

Group	Failure Torque (N·mm)	Failure Deformation (rad)	Energy to Failure (N·mm·rad)	Stiffness (N/mm)	n
NC	395.7 ± 33.2	0.18 ± 0.01	41.7 ± 4.5	2345.3 ± 167.8	15
OC	362.5 ± 26.8	0.21 ± 0.02	42.4 ± 3.3	2007.5 ± 167.8	14
O(0.25)	441.4 ± 11.7 [a]	0.23 ± 0.01	53.8 ± 3.3 [a]	2164.4 ± 110.4	15
O(0.5)	487.0 ± 31.0 [a]	0.22 ± 0.01	57.1 ± 4.7 [a]	2558.0 ± 227.7 [a]	12

Table 5.5: Torsion testing of AOD treated OVX rats femurs (unnormalized data).

[a] reflects a significance of $p<0.05$ vs. OC

Group	Shear Stress (MPa)	Shear Strain (%)	Energy to Failure (mJ/mm^3)	Shear Modulus (MPa)	n
NC	73.4 ± 7.6	2.6 ± 0.2	0.31 ± 0.03	3113.7 ± 311.9	15
OC	61.2 ± 4.2	2.9 ± 0.2	0.33 ± 0.03	2478.1 ± 212.0	14
O(0.25)	66.7 ± 3.4	3.4 ± 0.2 [b]	0.39 ± 0.03	2267.1 ± 211.9	15
O(0.5)	84.1 ± 5.8 [a]	3.1 ± 0.2	0.44 ± 0.03 [a]	3094.3 ± 302.1	12

Table 5.6: Torsion testing of AOD treated OVX rats femurs (normalized data).

[a] reflects a significance of $p<0.05$ vs. OC; [b] reflects a significance of $p<0.1$ vs. OC

5.3.3 Structure: Femoral Cross-Section

AOD induced changes in the structure of the femur. Although there were no significant differences in internal or external diameters, the lateral thicknesses of both O(0.25) and O(0.5) were significantly ($p<0.05$) higher than those of the OVX controls (Table 5.7;

Table 5.8). This was also true for the medial thickness of the O(0.25) group and there was an increasing trend ($p<0.1$) in the medial thickness of the O(0.5) group. There was also a significant ($p<0.05$) increase in the anterior thickness of the O(0.5) group.

Group	**Medial–Lateral**		**Posterior–Anterior**		**n**
	Outer Diameter (mm)	Inner Diameter (mm)	Outer Diameter (mm)	Inner Diameter (mm)	
NC	3.53 ± 0.07	2.38 ± 0.04	3.18 ± 0.05	1.97 ± 0.05	11
OC	3.64 ± 0.08	2.63 ± 0.10	1.97 ± 0.05	2.01 ± 0.07	10
O(0.25)	3.73 ± 0.08	2.51 ± 0.06	3.30 ± 0.06	2.10 ± 0.06	11
O(0.5)	3.63 ± 0.06	2.46 ± 0.06	3.24 ± 0.09	1.96 ± 0.06	12

Table 5.7: Diameters of AOD treated OVX rats femurs.

Group	**Lateral Thickness (mm)**	**Medial Thickness (mm)**	**Posterior Thickness (mm)**	**Anterior Thickness (mm)**	**n**
NC	0.57 ± 0.02	0.58 ± 0.03	0.52 ± 0.02	0.70 ± 0.02	11
OC	0.48 ± 0.02	0.52 ± 0.03	0.48 ± 0.03	0.64 ± 0.03	10
O(0.25)	0.59 ± 0.04 [a]	0.63 ± 0.02 [a]	0.53 ± 0.02	0.70 ± 0.02	11
O(0.5)	0.58 ± 0.03 [a]	0.58 ± 0.01 [b]	0.53 ± 0.03	0.74 ± 0.04 [a]	12

Table 5.8: Thicknesses of AOD treated OVX rat femurs.

[a] reflects a significance of $p<0.05$ vs. OC; [b] reflects a significance of $p<0.1$ vs. OC

5.3.4 Mineralization

Mineralization parameters were reflected with BSE and microhardness as discussed in section 3.3.4.

Back Scattered Electron Imaging

AOD did not affect the mineralization of cortical bone compared to OVX controls as was shown by the absence of significantly different BSE parameters (Table 5.9). This was also shown in the similar mineral distribution curves (Figure 5.3).

Group	Maximum Grey Level	Maximum Intensity (%)	Width at Half Maximum Intensity	Logit	n
NC	218.8 ± 3.3	2.4 ± 0.1	42.5 ± 2.6	-0.7 ± 0.2	13
OC	224.0 ± 4.1	2.5 ± 0.1	40.9 ± 4.7	-0.8 ± 0.2	12
O(0.25)	228.7 ± 6.2	2.6 ± 0.1	44.6 ± 2.6	-0.9 ± 0.2	11
O(0.5)	226.9 ± 3.5	2.6 ± 0.1	39.7 ± 1.3	-1.1 ± 0.1	12

Table 5.9: BSE imaging of cortical bone in the tibiae of AOD treated OVX rats.

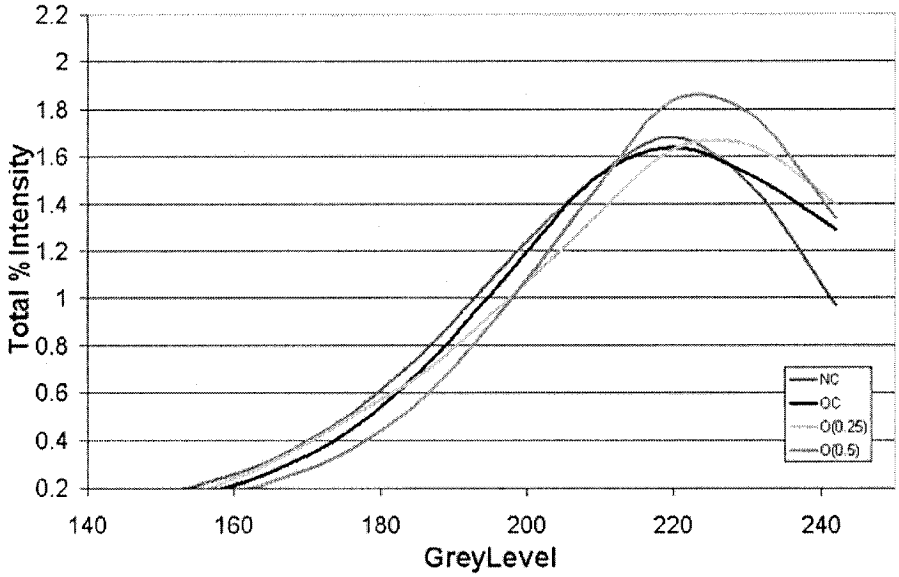

Figure 5.3: BSE distribution curves: comparing cortical bone mineralization in normal and OVX rats.

Microhardness

As in BSE testing, there was also an absence of significant differences in the hardness of cortical bone (Table 5.10). Once again this indicates no mineralization effects of AOD on OVX bone.

Group	Average Hardness (H)	n
NC	43.1 ± 0.6	13
OC	41.9 ± 0.4	14
O(0.25)	41.7 ± 0.5	12
O(0.5)	41.3 ± 0.6	13

Table 5.10: Hardness of cortical bone in AOD treated OVX rat tibia.

5.3.5 The Effect of AOD and OVX on Trabecular Bone

5.3.6 Bone Quantity: DXA

The effect of AOD and OVX on bone mineral density (BMD) and bone mineral content (BMC) was analyzed using Dual Energy X–Ray Absorptiometry (DXA). There were no significant differences between O(0.25), O(0.5) and OVX controls, which indicated that AOD treatment did not affect trabecular BMD or BMC (Figure 5.4; Table 5.11).

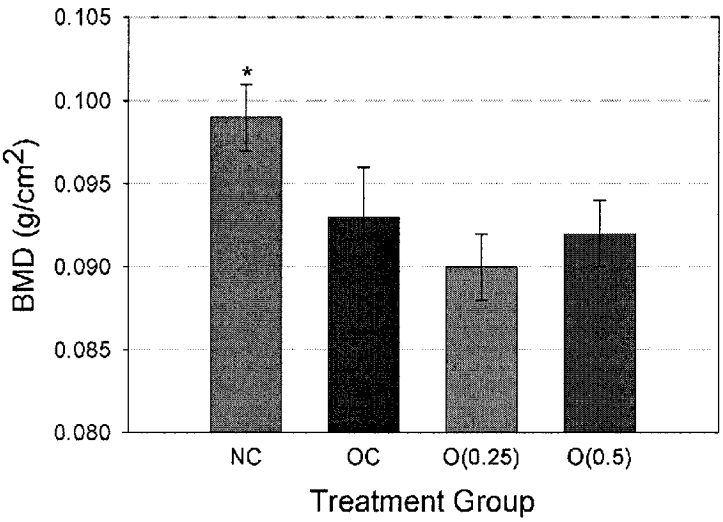

Figure 5.4: Vertebral BMD: comparing O(0.25) and O(0.5) with NC and OC groups

Group	BMD (g/cm^2)	BMC (g)	n
NC	0.099 ± 0.002	0.149 ± 0.004	11
OC	0.093 ± 0.003	0.136 ± 0.006	11
O(0.25)	0.09 ± 0.002	0.134 ± 0.005	9
O(0.5)	0.092 ± 0.002	0.137 ± 0.004	11

Table 5.11: Vertebral BMD and BMC of AOD treated OVX rats.

5.3.7 Mechanical Properties

Trabecular bone mechanical properties were determined through femoral neck fracture tests and vertebral compression. While femoral neck fracture reflects clinically significant properties, it is a less pure trabecular bone test than vertebral compression due to the mixture of cortical and trabecular bone as well as complex geometry in the neck region.

Femoral Neck Fracture

While there were no significant differences in the failure load between O(0.25), O(0.5) and OVX controls, the failure displacements of O(0.25) and O(0.5) were significantly ($p<0.05$) lower than the OVX controls (Table 5.12). Also, there was a decreasing trend in the energy to failure of O(0.25) compared to the OVX controls. These results indicate an increased fragility in the trabecular bone of the femoral neck due to AOD treatment.

Group	Failure Load (N)	Failure Displacement (mm)	Energy to Failure (mJ)	Stiffness (N/mm)	n
NC	176.7 ± 8.2	1.14 ± 0.08	90.7 ± 6.9	335.8 ± 16.2	14
OC	107.7 ± 5.8	0.51 ± 0.06	29.7 ± 3.4	264.5 ± 37.0	9
O(0.25)	108.6 ± 2.1	0.41 ± 0.02 [a]	24.5 ± 1.7 [b]	302.5 ± 13.1	10
O(0.5)	107.0 ± 3.2	0.41 ± 0.01 [a]	25.6 ± 1.4	301.4 ± 13.1	11

Table 5.12: Femoral neck fracture of the femurs of AOD treated OVX rats.
[a] reflects a significance of $p<0.05$ vs. OC; [b] reflects a significance of $p<0.1$ vs. OC

Vertebral Compression

The failure stress of O(0.25) was significantly ($p<0.05$) higher than that of the OVX controls (Table 5.14). The unnormalized and the normalized energy to failure of O(0.25)

were also significantly ($p<0.05$) higher (Table 5.13). This reflects an increased strength and toughness in OVX bone due to treatment with AOD–0.25. However, this was not true for treatment with AOD–0.5. Instead, this higher dose caused significantly higher stiffness and elastic modulus values only.

Group	Failure Load (N)	Failure Displacement (mm)	Energy to Failure (mJ)	Stiffness (N/mm)	n
NC	119.5 ± 3.9	0.41 ± 0.02	90.7 ± 6.9	330.8 ± 13.2	11
OC	145.1 ± 8.8	1.17 ± 0.14	71.0 ± 5.7	218.0 ± 19.8	11
O(0.25)	163.4 ± 8.8	1.31 ± 0.12	95.4 ± 9.7 [a]	265.2 ± 16.8	12
O(0.5)	151.6 ± 6.5	0.95 ± 0.09	72.3 ± 7.1	299.9 ± 27.5 [a]	13

Table 5.13: Vertebral compression of AOD treated OVX rat vertebrae (unnormalized data).

[a] reflects a significance of $p<0.05$ vs. OC

Group	Failure Stress (MPa)	Failure Strain (%)	Energy to Failure (MJ/mm^3Pa)	Elastic Modulus (MPa)	n
NC	17.8 ± 1.1	0.26 ± 0.02	2.1 ± 0.2	151.5 ± 9.7	14
OC	15.2 ± 1.1	0.27 ± 0.03	1.8 ± 0.2	98.6 ± 9.8	11
O(0.25)	17.7 ± 0.9 [a]	0.32 ± 0.03	2.5 ± 0.3 [a]	121.3 ± 9.8	12
O(0.5)	16.8 ± 0.9	0.23 ± 0.03	1.9 ± 0.3	142.7 ± 15.0 [a]	13

Table 5.14: Vertebral compression of AOD treated OVX rat vertebrae (normalized data).

[a] reflects a significance of $p<0.05$ vs. OC

5.3.8 Trabecular Structure and Connectivity Analysis

There was a significant ($p<0.05$) increase in the length of node-node struts in the O(0.25) group compared to the OVX controls (Table 5.16). There were no other significant differences between the AOD treated groups and the OVX controls.

However, in the O(0.25) group several structural and connectivity parameters were in between values of the OVX and normal contols. This was not true in the case of the O(0.5) group. While OVX decreased trabecular bone volume, trabecular thickness, trabecular number and the total length of the skeleton, these parameters were no longer significantly different when O(0.25) was compared to the normal controls (Table 5.15). Although the number of multiple points was still significantly lower than the normal controls, the numbers at least show that this parameter moved closer to the value of the normal control group. Also, there was a decreasing trend ($p<0.1$) in the length of node-node struts of O(0.25) compared to normal controls. However, the value is still significantly higher ($p<0.05$) than that of the OVX controls. Overall, this shows that AOD–0.25 at least partially prevented OVX-induced structural deterioration.

Group	Trabecular Bone Volume (%)	Average Trabecular Thickness (μm)	Trabecular Number	Trabecular Separation (μm)	n
NC	18.4 ± 1.8	71.4 ± 2.7	2.6 ± 0.2	358.3 ± 50.1	11
OC	12.3 ± 1.1 [c]	61.9 ± 2.1 [c]	2.0 ± 0.2 [c]	507.0 ± 71.7	13
O(0.25)	15.5 ± 1.9	65.7 ± 3.0	2.3 ± 0.2	403.5 ± 52.1	9
O(0.5)	13.7 ± 1.2 [c]	67.1 ± 2.5	2.0 ± 0.2 [c]	465.7 ± 55.4	11

Table 5.15: Trabecular structure in the proximal tibia of AOD treated OVX rats.

[c] reflects a significance of $p<0.05$ vs. NC

Group	Total Skeletal Length (mm/mm^2)	Node–Node Strut Length (mm/mm^2)	Node–Free Strut Length (mm/mm^2)	Free–Free Strut Length (mm/mm^2)	Multiple Points (#/mm^2)	n
NC	2.5 ± 0.3	0.9 ± 0.2	0.8 ± 0.1	0.3 ± 0.1	4.6 ± 0.8	11
OC	1.8 ± 0.2 [c]	0.2 ± 0.1 [c]	0.6 ± 0.1	0.6 ± 0.1	2.4 ± 0.3 [c]	13
O(0.25)	2.2 ± 0.3	0.5 ± 0.1 [ad]	0.8 ± 0.1	0.4 ± 0.1	3.1 ± 0.6 [c]	9
O(0.5)	1.9 ± 0.2 [c]	0.4 ± 0.1 [c]	0.6 ± 0.1	0.4 ± 0.1	2.3 ± 0.2 [c]	11

Table 5.16: Trabecular connectivity in the proximal tibia of AOD treated OVX rats.

[a] reflects a significance of $p<0.05$ vs. OC; [c] reflects a significance of $p<0.05$ vs. NC; [d] reflects a significance of $p<0.1$ vs. NC

5.3.9 Trabecular Remodeling: Histomorphometry

There were no significant differences in either the O(0.25) or the O(0.5) groups compared to the OVX controls. However, the values in the O(0.25) group were in between the normal controls and OVX controls as shown in Table 5.17. The osteoid surface of the OVX controls was significantly higher than that of the normal controls; however, the significance disappeared with AOD–0.25 treatment. This implies that AOD–0.25 may have prevented some of the OVX–induced increases in bone formation. Meanwhile, AOD–0.5 appeared to have the opposite effect. Osteoid volume, osteoid surface and osteoid volume/bone volume were even higher than the values of the OVX controls and therefore further from normal control values. The osteoid surface of the O(0.5) group was significantly higher than the normal controls. Therefore, AOD–0.5 appeared to increase bone formation compared to normal controls and perhaps even compared to the OVX controls.

Group	Osteoid Volume (%)	Osteoid Surface (%)	OV/BV (%)	n
NC	0.5 ± 0.1	7.7 ± 1.7	4.0 ± 1.1	13
OC	0.8 ± 0.13	16.4 ± 2.33 [c]	6.0 ± 1.0	11
O(0.25)	0.6 ± 0.1	13.9 ± 1.4	4.6 ± 0.7	13
O(0.5)	1.0 ± 0.1 [c]	20.9 ± 1.7 [c]	8.9 ± 2.4	10

Table 5.17: Histomorphometry parameters of AOD treated OVX rats.

[c] reflects a significance of $p<0.05$ vs. NC

5.3.10 Mineralization

Back Scattered Electron Imaging

Both doses of AOD prevented the OVX–induced decreases in mineralization as shown in Figure 5.5. O(0.25) and O(0.5) were shifted 7% and 6% respectively to higher grey levels as compared to OVX controls. The mineralization levels became similar to that of the normal controls. This shift was also reflected in the logit function which describes the shape of the distribution. As shown in Table 5.18, the logit function of both O(0.25) and O(0.5) were similar to that of the normal controls.

Group	Maximum Grey Level	Maximum Intensity (%)	Width at Half Maximum Intensity	Logit	n
NC	190.1 ± 3.1	1.6 ± 0.1	59.9 ± 2.6	0.8 ± 0.1	13
OC	178.0 ± 1.9 [c]	1.6 ± 0.1	59.3 ± 4.4	1.3 ± 0.1 [c]	11
O(0.25)	190.4 ± 5.5 [a]	1.7 ± 0.1 [b]	52.8 ± 1.8	0.7 ± 0.2 [a]	11
O(0.5)	189.2 ± 4.2 [b]	1.6 ± 0.1	59.5 ± 3.8	0.9 ± 0.2 [b]	11

Table 5.18: BSE imaging of trabecular bone in the proximal tibia of AOD treated OVX rats.

[a] reflects a significance of $p<0.05$ vs. OC; [b] reflects a significance of $p<0.1$ vs. OC; [c] reflects a significance of $p<0.05$ vs. NC

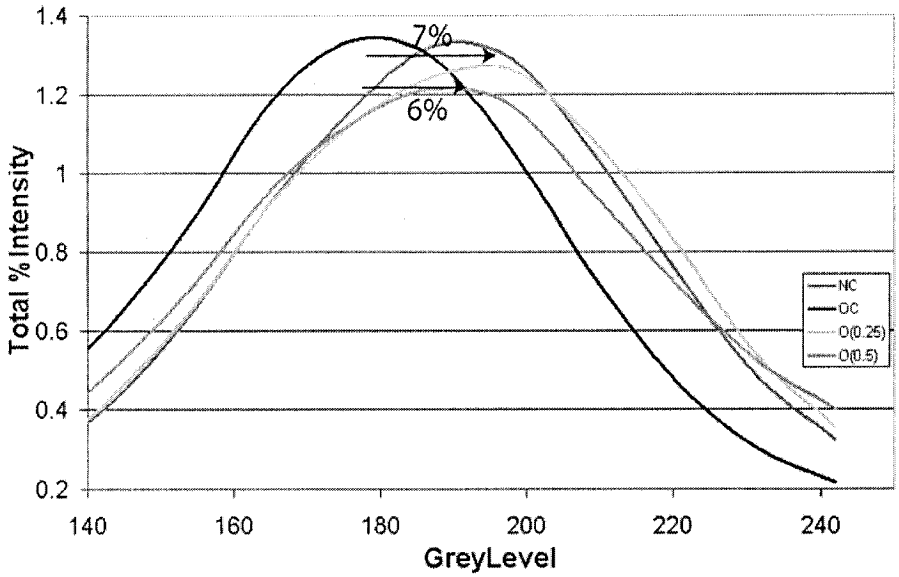

Figure 5.5: BSE distribution curves: comparing cortical bone mineralization in O(0.25), O(0.5), OC and NC groups

Microhardness

There were no significant differences in the hardness of the O(0.25) and O(0.5) groups compared to OVX Controls (Table 5.19).

Group	Average Hardness (H)	n
NC	39.3 ± 0.5	13
OC	38.7 ± 0.5	14
O(0.25)	37.9 ± 0.4	12
O(0.5)	38.0 ± 0.4	13

Table 5.19: Hardness of trabecular bone in AOD treated OVX rats.

5.4 Summary and Discussion of Results

Both AOD doses caused a 50% decrease in OVX–induced weight gain. In the skeleton, there were differences in both cortical and trabecular responses and these also appeared to be dose dependent.

Both doses increased the strength of cortical bone in torsion as evidenced by increased failure torque and energy to failure as well as failure strain in the case of AOD–0.25 and stiffness for AOD–0.5. In three point bending, results were not as clear but AOD–0.25 increased the failure load while AOD–0.5 increased failure load and stiffness but decreased the failure displacement. These increases in strength were accompanied by changes in bone quality and quantity. Both doses increased lateral and medial thicknesses as well as BMD.

In trabecular bone, neither dose appeared to increase vertebral BMD; nevertheless, this did not appear to compromise the strength of the trabecular bone in the vertebrae at least with AOD–0.25. In vertebral compression tests, AOD–0.25 increased failure stress and energy to failure thereby showing an increase in overall strength. AOD–0.5 caused a significantly higher stiffness and elastic modulus although this was not accompanied by increased stress or energy to failure. Furthermore, femoral neck fracture tests showed a decreased failure displacement with both doses along with a decreased energy to failure with AOD–0.25, which implies decreased toughness in this region.

In O(0.25) the strength increase appeared to be based on both structural and material properties. At the structural level, AOD–0.25 protected at least in part against OVX–induced bone loss. Therefore, there was more bone and importantly more connected bone. Additionally, histomorphometry revealed a decreased formation with AOD–0.25 compared to OVX contorls. The combination of structural and bone formation effects imply that AOD–0.25 may decrease the rate of remodeling compared to OVX. At the material level, AOD–0.25 caused an increase in mineralization. Curiously, these structural and mineral increases were not evident in BMD. This may may have been due to

limitations in the DXA technique and its resolution or in bone preparation.

Contrarily, in O(0.5), the increased stiffness and elastic modulus independent of other parameters was likely due to the increased mineralization without corresponding increases in structure. This lack of a structural change is likely due to an inability of AOD–0.5 to protect against OVX–induced remodeling increase. This was seen in the lack of structural changes in combination with slightly increased bone formation.

Chapter 6

Discussion

6.1 Skeletal Effect of OVX

The OVX model in this study behaved as expected from literature. Previous groups have also shown a decline in strength and stiffness in samples subjected to femoral neck fracture and vertebral compression tests (Bagi et al., 1997; Mosekilde et al., 1998; Turner et al., 1994). A decrease in trabecular BMD has also been reported (Baldock et al., 1999). Similarly, significant bone loss has been shown (Kalu, 1991; Wronski and Yen, 1991). As we saw in our study, this bone loss has been reported to be more pronounced in trabecular bone than cortical bone (Wronski and Yen, 1991; Baldock et al., 1999; Kalu, 1991). This bone loss has been associated with an increase in bone turnover (Shen et al., 1995; Morris et al., 1992). We can show an increase in bone turnover indirectly through a decrease in trabecular bone volume and an increase in bone formation. In this study, we found an increased bone formation as displayed by significantly higher osteoid surface. Other groups have also demonstrated increased bone formation due to OVX (Baldock et al., 1999).

6.2 Effect of AOD on Weight

While the OVX rats in this study gained 20% of their original body weight compared to the normal controls, AOD treatment caused a 50% decrease in this weight–gain. The magnitude of this prevention of weight–gain is similar to in vivo experiments assessing the lipolytic effects of AOD in either the Zucker (fa/fa) rat or the C57BL/6J (ob/ob) mouse despite differences in genetics, treatments and study duration. AOD orally administered to Zucker (fa/fa) rats at a level of 0.5 mg/kg/body weight over a period of 20 days reduced their weight gain over 50% compared to controls (Ng et al., 2000). Another study involving Zucker (fa/fa) rats placed slow–release tablets, designed to release 0.45 mg/kg/day, under a skin layer in the abdomen for a 20 day period and noted a significant decrease in weight–gain by day 8 (Ng et al., 2000b). An earlier study looked at the effect of 0.2 mg/kg/day dosed via an intraperitoneal injection for 18 days in the C57BL/6J (ob/ob) mouse and noted an average decrease in weight gain of approximately 27% compared to controls (Natera et al., 1994). Therefore, our study indicates that AOD is successful at decreasing the OVX–induced weight gain just as it has previously been shown to do in leptin deficient or leptin receptor deficient rodent models. Therefore, the AOD-induced decrease in weight gain that was evidenced in the OVX model of this study correlates to the AOD-induced weight loss seen in the obese models of previous studies. Nevertheless, the mechanisms responsible for the weight-loss remain unclear. It has been suggested that AOD's weight effects are controlled by an upregulation of the β_3–adrenergic receptors (Atgie et al., 1997), which activates the G protein signalling pathway and causes stimulation of hormone-sensitive lipase (Hollenga et al., 1991). However, it has also been shown that there is no direct mediation through the growth hormone receptors, which indicates that the activation may occur indirectly (Heffernan et al., 2001a).

6.3 Skeletal Effect of AOD

6.3.1 A Comparison of the Effects of Growth Hormone and AOD

The intact growth hormone, as reported from previous studies, has a similar effect on the rat skeleton as did AOD in our study. In normal bone, studies have shown that the effect of growth hormone is more significant in cortical bone than in trabecular bone. Increases in femoral BMD and thicknesses have been reported (Andreassen et al., 1996; Jorgensen et al., 1991). In our study we also saw significant femoral BMD increases with AOD–0.5 and a non–significant increase in the medial–lateral thickness although these increases were not evident with AOD–0.25. This indicates that dose is important in the response as discussed below. In three point bending tests, studies have shown increases in ultimate load although no effect on stress and elastic modulus (Mosekilde et al., 1999). We also saw increases in the failure load with AOD–0.5 and an absence of effects on stress and elastic modulus. In three point bending tests, AOD–0.25 did not produce any significant effects. Meanwhile, in trabecular bone subjected to growth hormone studies have shown that there were no significant increases in vertebral or femoral neck strength (Andreassen et al., 1996), which was also evident in our study with both doses. Furthermore, histological studies reveal that growth hormone does not significantly increase trabecular bone volume (Gunness and Hock, 1995), which we also demonstrated. This histological study also indicates that there is no increase in bone formation rate with growth hormone. While we were not able to study rate we did see an increase in bone formation in our study with AOD-0.25. This discrepancy may be a result of comparing static and dynamic parameters or may also arise from the fact that the study by Gunness and Hock used 18 month old rats whereas we studied 6-9 month old rats. Older rats are known to have less bone formation than younger rats. The similarities between growth hormone studies and our AOD study are also apparent in

OVX bone. In cortical bone, growth hormone has been shown to increase the bone mass compared to OVX controls (Verhaeghe et al., 1996; Wang et al., 2001) which we also saw with both AOD doses through BMD studies. We also saw this in terms of increased femoral thicknesses. Three point bending tests have shown that growth hormone increases ultimate load of the femur but has no effect on stress or elastic modulus (Andreassen and Oxlund, 2000; Mosekilde et al., 1998). While we saw this failure load increase with both AOD doses we also saw increases in stiffness and stress with AOD–0.5. In trabecular bone, studies have shown an increase in vertebral strength although not in ultimate stress or elastic modulus (Andreassen et al., 1996). We also saw increases in failure stress with AOD–0.25 but also saw an increased energy to failure with this dose and an increase in stiffness and elastic modulus with AOD–0.5.

Overall, there is a similarity between growth hormone and AOD effects on the skeleton. However, one obvious discrepancy arises in effective doses. Studies in aged rats in OVX bone have shown significant effects only with growth hormone doses greater than 2mg/kg/day (Mosekilde et al., 1998). Meanwhile, in our study we have shown similar responses with much lower doses (0.25 mg/kg/day and 0.5 mg/kg/day). Furthermore, previous work from our lab on the skeletal effect of AOD in the OVX rat tested 0.75 mg/kg/day and 2.0 mg/kg/day and found that these doses did not produce significant skeletal effects. Therefore, it appears that the growth hormone peptide, AOD, is more potent than the intact growth hormone. A similar result has also been shown in lipolytic studies in which a lower molar dose of AOD9604 has been shown to elicit the same lipolytic effect as the intact hGH (Ng et al., 2000b).

6.3.2 The Dose Dependency of AOD

Our study revealed strong dose dependent differences in the skeletal effect of AOD such that AOD–0.25 was more effective at protecting against OVX–induced bone loss than AOD–0.5. This indicates that AOD–0.5 may be too high a dose. It is possible that

too much AOD saturates the operating system and instigates a negative feedback cycle. However, we must consider these two doses as part of a spectrum as revealed in a dose study that was performed in parallel. This study looked at the skeletal effects of 1, 3, 10, 30, 100 and 300 μg AOD/kg/day (unpublished data). Before drawing a comparison it must first be noted that there were some obvious differences in this study and ours. There is a contrast in the age differences in the animals (3 months vs. 6–9 months), the sample sizes, the parameters reported (maximum values vs. failure values) and the vertebral compression methods. Nevertheless, data was normalized to provide a percentage of protection value, which allows for comparison with our study. A comparison reveals that AOD has maximum protective effects against OVX-induced fragility at 1 and 250 μg/kg/day. this indicates a bimodal activity of AOD, which may result from a combination of stimulatory and inhibitory effects.

6.3.3 Possible Mechanisms of AOD

We have shown that the skeletal effects of AOD are complex in that they differ in normal and OVX bone as well as in cortical and trabecular bone and there was also a dose dependency. We can speculate that AOD may be anabolic to bone based on similarities to growth hormone, which has been shown to promote osteoblast proliferation and differentiation (Morel et al., 1993; Kassem et al., 1993) and to be anabolic to the skeleton (Baroncelli et al., 2003). We also saw that AOD–0.25 promoted cortical bone formation in OVX bone and trabecular bone formation in normal trabecular bone. However, this was a preventative study rather than a treatment study and therefore further studies will have to assess whether or not AOD is in fact anabolic. For now, however, we can speculate on some possible mechanisms for the skeletal effect of AOD through an examination of molecules that have known effects on fat, bone or both.

Insulin-like growth factor

The insulin–like growth factor (IGF) mediates many of the growth hormone's actions

(Canalis, 1995; Clark, 1997; Marcus, 1997; Rosen, 1994)). Therefore, it is possible that the GH peptide, AOD, indirectly stimulated IGF production. Rat osteoblasts have been shown to produce IGF–I with regulation by the growth hormone, parathyroid hormone and other growth factors and interleukins (Conover, 1996). In turn, IGF-I has been shown to regulate bone formation both systemically and locally (Baylink, 1993; Rosen, 1995). Osteoclasts have also been shown to produce IGFs and it has been speculated that the local production of IGFs by osteoblasts and osteoclasts regulates the coupling of bone formation to bone resorption (Mohan and Baylink, 1999). Furthermore, low doses of IGF–I have been shown to increase bone formation greater than the increases in bone resorption, causing a net increase in bone mass (Marcus, 1997). In this manner, if AOD does in fact stimulate IGF production then this could explain the attenuation of bone formation and bone loss that was observed. Furthermore, since growth hormone has been shown to be more anabolic to cortical than trabecular bone this may explain the more significant cortical effects that were observed along with the lack of trabecular effects in the normal bone. Additionally, exogenous IGF–I has been shown to decrease growth hormone secretion in animals and humans thereby having a negative feedback role, which could explain the dose-dependency of AOD (Guler, 1987; Bermann, 1994)).

Estrogen

The best known effect of OVX is a decrease in sex hormones of which estrogen is a major player. This decreased hormone level has been shown to increase the production of osteoclastogenic cytokines and to decrease the expression of inhibitory factors for osteoclastogenesis resulting in a suppression of osteoclastic bone resorption (Manolagas and Jilka., 1995, Spelsberg et al., 1999; Saika et al., 2001). The effect of estrogen on bone formation is less clear; however, estrogen has been identified as a possible promoter of osteoblast differentiation (Okazaki et al., 2002). In this manner, decreased estrogen levels decrease bone formation, as we saw in the OVX model of our study.

Additionally, it has also been shown that estrogen-induced increases in osteoblast

differentiation occur at the expense of adipocyte differentiation (Okazaki et al., 2002). Osteoblasts and adipocytes are both of mesenchymal origin stemming from progenitor bone marrow stromal cells (Okazaki et al., 2002). An inverse relationship between osteoblastogenesis and adipogenesis has been indicated based on observed increases in lipid accumulation in bone marrow in association with age-related bone loss (Burkhardt et al., 1987; Nuttall et al., 2000; Gimble et al., 1996) and ovariectomy induced bone loss (Martin et al., 1990). Okazaki et al. studied the effects of estrogen in vitro in mouse cells on BMP-2 induced osteoblatogenesis and adipogenesis and found that estrogen directly modulated bipotential stromal cell differentiation and caused a lineage shift towards osteoblasts rather than adipocytes. The group postulated that this would in turn directly stimulate bone formation although the molecular mechanism remains unknown (Okazaki et al., 2002). Interestingly; however, this possible effect on fat and bone reflects the same inverse relationship that we saw in our study. We saw increased fat and decreased bone mass with OVX but also decreased fat and increased bone mass with AOD treatment. This brings into consideration a possibility of AOD increased estrogen levels thereby causing the evidenced fat loss and bone gain. This may be possible since estrogen has been shown to influence bone indirectly through the growth hormone by IGF-I as previously discussed. However, estrogen effects could not account for the observed increases in normal bone. Furthermore, while a relationship between growth hormone and estrogen have been identified, it is unclear whether the interaction is synergistic (Slootweg et al., 1997; Suliman et al., 2001) or antagonistic (Leung et al., 2003).

Leptin

Leptin is a hormone produced by adipocytes that acts like a thermostat to control the body's fat load. An increase in circulating leptin suppresses a hypothalamic peptide, which suppresses eating (Whitfield, 2001). There is also some evidence of a direct effect of leptin on adipose tissue. Leptin-treated adipose tissue has been shown to incease glucose utilization and lipolysis (Siegrist-Kaiser et al., 1997). Recently, leptin has also

been identified for its possible role in bone regulation. Leptin receptors are expressed on bone cells (Cornish et al., 2002; Reseland et al., 2001) and leptin has been shown to have direct effects on osteoblast proliferation (Cornish et al., 2002), maturation (Thomas et al., 1999), osteoclast development (Cornish et al., 2002, Holloway et al., 2002) and chondrocyte activity (Cornish et al., 2002). However, the nature of these skeletal effects is a subject of much debate.

Karsenty's group examined a leptin deficient mouse. They hypohesized that leptin deficiency would cause low circulating leptin levels, which would in turn cause low estrogen levels and induce low bone mass. However, they found that leptin deficiency actually increased bone mass. Intracerebroventricular leptin injections decreased bone mass (Karsenty, 2000). When they examined this result at the cellular level, they found an increase in osteoclast function as expected due to the decreased estrogen levels but they also noticed a much greater number of osteoblasts. Karsenty's group also showed that leptin deficient and leptin receptor deficient mice have higher spinal trabecular bone volume, which indicates an inverse relationship between leptin and bone mass (Ducy et al., 2000; Takeda et al., 2002).

Reid and Burguera suggest that these trabecular effects are primarily controlled by central regulation (Reid, 2004; Burguera et al., 2001). In this manner, circulating leptin may bind to receptors on the hypothalamus and signals then stimulate the expression of hypothalamic osteoblast inhibitory factor. However, a decrease in either leptin or leptin receptors would cause a reduction in this inhibitory factor and thereby cause an increase in osteoblast productivity (Baldock et al., 2001). This could explain the increases in spinal trabecular bone volume that were shown in our study. AOD decreased the amount of fat, which could have decreased leptin levels and following the above argument, an increased osteoblast productivity and this could have produced the increases in trabecular bone volume and bone formation that we showed.

However, there is also evidence that leptin levels and bone are positively correlated.

The leptin deficient mouse has been shown to have decresed total, diaphyseal, distal and metaphyseal BMD, decreased total femoral calcium content and increased femoral fragility (Mathey et al., 2002). Similarly, leptin deficient mice have also been shown to have reduced femoral length and BMC (Steppan et al., 2000). In this latter case, intraperitoneal leptin injections inceased the bone area. Leptin has also been shown to increase endocortical bone formation in the mouse (Liu et al., 1997), and to increase bone strength and promote IGF-I mediated endochondral bone formation in the rat (Cornish et al., 2001).

To explain these results, Reid and Burguera suggest that leptin defieciency decreases cortical bone through direct effects (Reid, 2004; Burguera et al., 2001). Leptin has been shown to suppress osteoclast activity though OPG and RANKL and to promote osteoblast activity through stimulation of IGF–I. In this manner, a decease in leptin reduces the direct anabolic effects of leptin on osteoblasts and its precursors as well as an inhibition of osteoclastogenesis (Reid, 2004). This may promote bone loss in cortical bone and trabecular bone although Reid suggests that the abundance of cortical effects may be a result of regional differences according to bone marrow type and bone innervation. When we consider this in the context of our study, however, we see a contradiction. AOD prevented OVX induced weight-gain, which likely led to decreases in leptin but we did not see cortical thinning but in fact the opposite, which may be due to the magnitude of the effect. We previously discussed the possibility that AOD stimulated IGF–I (based on the growth hormone effects) independent of leptin and the IGF-induced improvements may be larger than the leptin modulated effect.

6.4 Limitations of the study

6.4.1 BMD testing

According to vertebral BMD tests, AOD did not improve trabecular bone mineral density; however, bone quality tests revealed that AOD-0.25 increased mineralization and decreased bone loss compared to OVX controls. This discrepancy may have resulted from reduced sample size in the BMD tests or dissection damage. Vertebrae have strongly attached pedicles, which are difficult to remove without damaging the bone. In this study, if the damage was too significant, the vertebrae were exluded from the analysis, which reduced the sample size. Inclusion of slightly damaged samples may have influenced BMC values to appear artificially lower. To try and account for this, within this study, BMD values were relied on more heavily than BMC values. In future, vertebral BMD measurements should be made within the spine before excision or at least on the roughly excised bones before the pedicles are trimmed for vertebral compression. Recently, we have tested this technique and shown a higher degree of precision (unpublished data).

In the femoral BMD tests of the OVX groups, there was high variability. This variability may have been a result of an inability to differentiate between cortical and trabecular regions in the bone. To avoid this in future, microCT could be used instead or in addition to the BMD tests. MicroCT provides a three–dimensional image of the bone which the user can then manipulate to isolate cortical and trabecular regions and analyze the BMD. This technique also provides a volumetric density which is more accurate than the arial density that DXA provides. This may be particularly useful for these studies since it was apparent that there were significantly different cortical and trabecular effects. Nevertheless, the BMD testing was generally capable of reporting trends that were also seen in mechanical and bone quality tests.

6.4.2 Microhardness Testing

Another limitation of this study was the discrepancy in the mineralization shown through BSE and microhardness tests. While BSE showed decreases in mineralization due to OVX and prevention of this with AOD, the AOD improvments were not evident with microhardness testing. In trabecular bone this was likely due to edge effects and penetration. Even though the indenter was targeted in the middle of each trabeculae, the edge of the indent ended up being very close to trabecular edges. Also, it was difficult to judge whether the indentation completely penetrated trabeculae into the spur resin beneath. To try to account for these limitations in this study, outlying points were excluded; however, to obtain more precise microhardness data in future, microhardness tests could be performed with a narrower indenter such as the Knoop indenter or a lower load.

6.5 Conclusions

1 AOD prevented OVX-induced weight-gain.

2 Effects of AOD were site-specific and dose-dependent.

3 In normal bone, cortical effects were more pronounced than trabecular effects.

4 In normal bone, both AOD doses improved cortical strength.

5 In normal bone, AOD-0.25 increased bone formation.

6 AOD-0.25 prevented OVX-induced bone loss and fragility in cortical bone and decreased these parameters in trabecular bone.

7 AOD-0.5 prevented OVX-induced bone loss and fragility in cortical bone but not trabecular bone.

6.6 Future Work

This study opens the possibility that AOD may be anabolic to bone. Future studies should assess this in view of an osteoporosis treatment. This could be performed by waiting for a set period of time following ovariectomy before commencing dosages. Doses of 0.25 μg/kg/day and 0.001 μg/kg/day should be tested as they appeared to have the most protective capacity in both this study and a parallel study (unpublished data).

Chapter 7

References

Amprino R. 1961. Microhardness testing as a means of analysis of bone tissue biophysical properties. In: Biomechanical Studies of the Musculo-Skeletal System. FG Evans, ed. Charles C Thomas, Publisher, Springfield IL. pp.20–48.

An YH, Moreira PL, Kang QK, and Gruber HE (2003) Principles of Embedding and Common Protocols. In: An YH and Martin KL, eds. Handbook of Histology Methods for Bone and Cartilage. New Jersey: Humana Press Inc. pp 185–198.

Andreassen TT, Melsen F, and Oxlund H (1996) The influence of growth hormone on cancellous and cortical bone of the vertebral body in aged rats. *J. Bone Miner. Res.* **11**:1094–1102.

Andreassen TT and Oxlund H (2000) The influence of combined parathyroid hormone and growth hormone treatment on cortical bone in aged ovariectomized rats. *J. Bone Miner. Res.* **15**:2266–2275.

Atgie C, D'Allaire F, Bukowiecki LJ (1997) Role of β_3- and β_1-adrenergic receptors in

adipose tissue of congenitally obese (C57BL/6J ob/ob) mice. *Mol. Endocrinol.* **8**:518–527.

Bagi CM, Ammann P, Rizzoli R, and Miller SC (1997) Effect of estrogen deficiency on cancellous and cortical bone structure and strength of the femoral neck in rats. *Calcif. Tissue Int.* **61**:336–344.

Baldock PA, Need AG, Moore RJ, Durbridge TC, and Morris HA (1999) Discordance between bone turnover and bone loss: effects of aging and ovariectomy in the rat. *J. Bone Miner. Res.* **14**:1442–1448.

Baldock PA, Thomas GP, Sainsbury A, et al. (2001) Neuropeptide Y2 receptor has a role in the bone homeostasis independent of body weight. *J. Bone Miner. Res.* **16(suppl1)**: S141.

Baroncelli GI, Bertelloni S, Sodini F, and Saggese G (2003) Acquisition of bone mass in normal individuals and in patients with growth hormone deficiency. *J. Pediatr. Endocrinol. Metab.* **16** Suppl 2:327–35.

Baylink DJ, Finkelman RD, Mohan S (1993) Growth factors to stimulate bone formation. *J. Bone Miner. Res.* **8**(Suppl. 2):S564–S572.

Behncken SN and Waters MJ (1999) Molecular recognition events involved in the activation of growth hormone receptor by growth hormone. *J. Mol. Recog.* **12**: 355–362.

Bermann M, Jaffer CA, Tsai W, DeMott-Frieberg R, Barkan AL (1994) Negative feedback regulation of pulsatile growth hormone secreation by insulin-like growth factor-I.

Involvement of hypothalamic somatostain. *J. Clin. Invest.* **94**:138–145.

Bornstein J, Ng FM, Heng D and Wong KP (1983) Metabolic actions of pituitary growth hormone. Inhibition of acetyl CoA carboxylase by human growth hormone and a carboxyl terminal part sequence acting through a second messenger. *Acta. Endocrinologica* **103**:479–486.

Boyce TM, Tloebaum RD, Bachus KN, Skedros JG (1990) Reproducible method for calibrating the backscattered electron signal for quantitative assessment of mineral content in bone. *Scan. Micros* **4**:591–603.

Bracci PM, Bull SB, Grynpas MD. (1998) Analysis of Compositional Bone Density Data Using Log Ratio. *J. Bone Miner. Res.* **9**:715–724.

Brummer RJM and Bengtsson BA (1995) The effect of growth hormone on body composition. *Asia Pascific Journal of Clinical Nutrition* **4**:151–155.

Burguera B, Hofbauer LC, Thomas T, Evans FGGL, Khosla S, Riggs BL, Turner RT (2001) Leptin reduces ovariectomy-induced bone loss in rats. *Endocrinology* **142**:3546–3553.

Burkhardt R, Kettner G, Bohm W, Schmidmeier M, Schlag R, Frisch B, Mallmann B, Eisenmenger W, Gilg T (1987) Changes in trabecular bone, hematopoiesis and bone marrow vessels in aplastic anemia, primary osteoprosis, and old age: a comparative histomorphometric study. *Bone* **8**: 157–164.

Burnell JM, Teubner EJ, and Miller AG (1980) Normal maturational changes in bone

matrix, mineral, and crystal size in the rat. *Calcif. Tissue Int.* **31**:13–19.

Canalis, E. (1995) Growth hormone, skeletal growth factors and osteoporosis. *Endocr. Pract.* **1**:39–43.

Carlstrom D (1954) Microhardness measurements on single haversian systems in bone. *Experientia* **10**:171.

Carrel AL and Allen DB (2000) Effects of growth hormone on body composition and bone metabolism. *Endocrine* **12**:163–172.

Carro E, Senaris R, Considine RV, Casanueva FF, Dieguez C (1997) Regulation of in vivo growth hormone secretion by leptin. *Endocrinology* **138**:2203–2206.

Carter-Su C, Schwartz J, Smit LS (1996) Molecular mechanisms of growth hormone action. *Annu. Rev. Physiol.* **58**:187–207.

Chretien M (1999). Clinical relevance of convertases: atherosclerosis, Alzheimer's disease, obesity, diabetes and HIV. *Clinical Investigative Medicine* **22**:207–211.

Clark R. (1997). Growth hormone and insulin-like growth factor 1: New endocrine therapies in cardiology. *Trends Cardiovasc. Med.* **7**:264–268.

Compston JE, Garrahan NJ, Croucher PI, Wright CD, and Yamaguchi K (1993) Quantitative analysis of trabecular bone structure. *Bone* **14**:187–192.

Copeland KC and Nair KS (1994) Acute growth hormone effects on amino acid and

lipid metabolism. *J. Clin. Endocrinol. Metab.* **78**:1040–1047.

Cornish J, Callon KE, Bava U, et al (2001) The direct actions of leptin on bone cells increase bone strength in vivo: an explanation of low requency fracture rates in obesity. *Bone* **28**:S88.

Cornish J, Callon KE, Bava U, Lin C, Naot D, Hill BL, et al (2002) Leptin directly regulates bone cell function in vitro and reduces bone fragility in vivo. *J. Endocrinol.* **175**:405–415.

Costoya JA, Finidori J, Moutoussamy s, Senaris R, Devesa J, Arce VM (1999) Activation of growth hormone receptor delivers an antiapoptotic signal: evidence for a role of Akt in this pathway. *Endocrinology* **140**:5937–5943.

Council of the National Osteoporosis Foundation (1996) Guidelines for the early detection of osteoporosis and prediction of fracture risk. *S. Afr. Med. J.* **86**:1113–1116.

Cowell CT and Dietsch S (1995) Adverse events during growth hormone therapy. *J. Pediatr. Endocrinol. Metab.* **8**:243–252.

Cunningham BC, Jhurani P, Ng P, and Wells JA (1989) Receptor and antibody epitopes in human growth hormone identified by homolog–scanning mutagenesis. *Science* **243**:1330–1336.

Currey JD, Brear K (1990) Hardness, Young's modulus and yield stress in mammalian mineralized tissues. *J. Mater. Sci.: Mater. Med.* **1**:14–20.

Daughaday WH and Rotwein P. Insulin-like growth fators I and II (1989) Peptide, messenger ribonucleic acid and gene structures, serum and tissue concentrations. *Endocr. Rev.* **10**:68–91.

De Laureto PP, Toma S, Tonon G, and Fontana A (1995) Probing the structure of human growth hormone by limited proteolysis. *Int. J. Peptide Protein Res.* **45**:200–208.

De Vos AM, Ultsch M, and Kossiakoff AA (1992) Human growth hormone and extracellular domain of its receptor: crystal structure of the complex. *Science* **255**:306–312.

Dietz J and Schwartz J. Growth hormone alters lipolysis and hormone–sensitive lipase activity in 3T3–F442A adipocytes. *Metabolism* **40**: 800–806.

Ducy P, Amling M, Takeda S, Priemel M, Schilling AF, Beil F, et al (2000) Leptin inhibits bone formaition through a hypothalamic relay: a central control of bone mass. *Cell* **100**:197–207.

Eastell R, Delmas PD, Hodgson SF, Eriksen EF, Mann KG, and Riggs BL (1988) Bone formation rate in older normal women: concurrent assessment with bone histomorphometry, calcium kinetics, and biochemical markers. *J. Clin. Endocrinol. Metab.* **67**:741–748.

Effendi W and Ng FM (1993) Effect of an anti-lipogenic fragment of human growth hormone on glucose transport in rat adipocytes. *Biochem. Mol. Bio. Int.* **31**:543–552.

Erikson EF, Axelrod DW, and Melson F. 1994. Bone Histomorphometry. New York: Raven Press.

Evans GP, Behiri JC, Currey JD, Bonfield W (1990) Microhardness and Young's modulus in cortical bone exhibiting a wide range of mineral volume fractions, and in a bone analogue. *J. Mater. Sci.: Mater. Med.* **1**:38–43.

Foldes J, Shih MS, Levy J (1992) Bone structure and calcium metabolism in obese Zucker rats. *Int. J. Obes. Relat. Metab. Disord.* **16**:95–102.

Fisker S, Vahl N, Hansen TB, Jorgensen JO, Hagen C, Orskov H, Christiansen JS (1997). Serum leptin is increased in growth hormone-deficient adults: relationship to body composition and effects of pacebo-controlled growth hormone therapy for 1 year. *Metab. Clin. Exp.* **47**:812–817.

Gala PJ, Diaz-Curiel M, de la Piedra GC, Castilla RC, and Torralbo GM (1998) Bone mass assessment in rats by dual energy X–ray absorptiometry. *Br. J. Radiol.* **71**:754–758.

Garrahan NJ, Mellish RW, and Compston JE (1986) A new method for the two–dimensional analysis of bone structure in human iliac crest biopsies. *J. Microsc.* **142** (Pt3):341–349.

Gertner JM (1993) Effects of growth hormone on body fat in adults. *Horm. Res.* **40**:10–15.

Gimble JM, Robinsopn CE, Wu X, Kelly KA (1996) The function of adipocytes in the bone marrow stroma: an update. *Bone* **19**:421–428.

Goodman V and Hirsch J (1968) Multiple effects of growth hormone on lipolysis. *J. Clin. Endocrinol.* **2**:551–555.

Griffen MG, Kimble R, Hopfer W, and Pacifici R (1993) Dual–energy x–ray absorptiometry of the rat: accuracy, precision, and measurement of bone loss. *J. Bone Miner. Res.* **8**:795–800.

Grynpas MD, Acito A, Dumitriu M, Mertz B, Very J (1992) Changes in bone mineralization and mechanical properties due to long–term (1 year) administration of pamidronate (APD) to adult dogs. *Osteopor. Int.* **2**:74–81.

Grynpas MD, Holmyard DP, Pritzker KPH (1994) Bone mineralization and histomorphometry in biopsies of osteoporotic patients treated with fluoride. *Cells Mater.* **4**:287–297.

Guler HP, Zapf J, Froesch ER (1987) Short-term metabolic effects of recombinant human insulin-like growth factor I in healthy adults. *N. Engl. J. Med.* **317**:317–140.

Gunness M and Hock JM (1995) Anabolic effect of parathyroid hormone is not modified by supplementation with insulin–like growth factor I (IGF–I) or growth hormone in aged female rats fed an energy–restricted or ad libitum diet. *Bone* **16**:199–207.

Hansson T, Roos B, and Bachemson A (1980) The bone mineral content and ultimate compressive strength of lumbar vertebrae. *Spine* **5**:46–55.

Heany RP (1993) Is there a role for bone quality in fragility fractures? *Calcif. Tissue Int. Suppl.* **1**:S3–S6.

Heffernan MA, Jiang WJ, Thorburn AW, Ng FM (2000) Effects of oral administration

of a synthetic fragment of human growth hormone on lipid metabolism. *Am. J. Phsiol. Endocrinol. Metab.* **279**:E501–E507.

Heffernan MA, Thorburn AW, Fam B, Summers R, Conway-Campbell B, Waters MJ and Ng FM (2001a) Increase of fat oxidation and weight loss in obese mice caused by chronic treatment with human growth hormone or a modified C–terminal fragment. *Intl. J. Obesity* **25: 1442–1449**.

Heffernan M, Summers RJ, Thorburn A, Ogru E, Gianello R, Jiang WJ, Ng FM (2001b) The Effects of Human GH and Its Lipolytic Fragment (AOD9604) on Lipid Metabolism Following Chronic Treatment in Obese Mice and β_3–AR Knock–Out Mice. *Endocrinology* **142**:5182–5189.

Ho KK, O'Sullivan AJ, Hoffman DM (1996) Metabolic actions of growth hormone in man. *Endocr. J.* **43**(Suppl.): S57–S63

Hollenga C, Brouwer F and Zaagsma J (1991) Relationship between lipolysis and cyclic AMP generation mediated by atypical $\beta-$adrenoceptors in rat adipocytes.*Br. J. Pharmacol.* **102**:577–580.

Holloway WR, Collier FM, Aitken CJ, Myers DE, Hodge JM, Malakellis M, et al (2002) Leptin inhibits osteoclast generation. *J. Bone Miner. Res.* **17**:200–209.

Isgaard J, Nilsson A, Lindahl A, Jansson JO, and Isaksson OG (1986) Effects of local administration of GH and IGF–I on longitudinal bone growth in rats. *Am. J. Physiol.* **250**:E367-E372.

Issaksson OG, Eden S, Jansson JO (1985) Mode of action of pituitary growth hormone on target cells. *Annu. Rev. Physiol.* **47**:483–499.

Jorgensen PH, Bak B, and Andreasson TT (1991) Mechanical properties and biochemical composition of rat cortical femur and tibia after long–term treatment with biosynthetic human growth hormone. *Bone* **12**:353-359.

Jorgensen JO, Muller J, Moller J, Wolthers T, Vahl N, Juul A, Skakkebaek NE, and Christiansen JS (1994) Adult growth hormone deficiency. *Horm. Res.* **42**:235–241.

Kagi H, Sugimoto T, Kanatani M, Nishiyama K, Nasu M, and Chihara K (1997) Insulin–like growth factor–I mediates osteoclast–like cell formation stimulated by parathyroid hormone. *J. Cell Physiol.* **172**:55–62.

Kalu DN, Liu CC, Hardin RR, and Hollis BW (1989). The aged rat model of ovarian hormone deficiency bone loss. *Endocrinology* **124**:7–16.

Kalu DN (1991) The ovariectomized rat model of postmenopausal bone loss. *Bone Miner.* **15**:175–191.

Kaplan FS, Hayes WC, Keaveny TM, Boskey A, Einhorn TA, and Iannotti JP (1994) Form and Function of Bone. In:Simon SR, editor. Orthopaedic Basic Science. American Academy of Orthopaedic Surgeons. P 127–184.

Karsenty G. (2000) Teh central regulation of bone remodeling. *Trends Endocrinol Metab.* **11**:437–439.

Kassem M, Blum W, Ristelli J, Mosekilde L, and Eriksen EF (1993) Growth hormone stimulates proliferation and differentiation of normal human osteoblast–like cells in vitro. *Calcif. Tissue Int.* **52**:222–226.

Kato Y, Murakami Y, Sohmiya M, and Nishiki M (2002) Regulation of human growth hormone secretion and its disorders. *Intern. Med.* **41**:7–13.

Kelly PA, Goujon L, Sotiropoulos A, Dinerstein H, Esposito N, Edery M, Finidori J and Postel-Vinay MC (1994) The growth hormone receptor and signal transduction. *Hormone Research* **42**:133–139.

Kinney JH, Ryaby JT, Haupt DL, and Lane NE (1998) Three–dimensional in vivo morphometry of trabecular bone in the OVX rat model of osteoporosis. *Technol. Health Care* **6**:339–350.

Lane NE, Haupt D, Kimmel DB, Modin G, and Kinney JH (1999) Early estrogen replacement therapy reverses the rapid loss of trabecular bone volume and prevents further deterioration of connectivity in the rat. *J. Bone Miner. Res.* **14**:206–214.

Leichter I, Margulies JY, Weinreb A, Mizrahi J, Robin GC, Conforty B, Makin M, and Bloch B (1982) The relationship between bone density, mineral content , and mechanical strength in the femoral neck. *Clin. Orthop.* 272–281.

Leung KC, Doyle N, Ballesteros M, Sjogren K, Watts CK, Low TH et al. (2003) Estrogen inhibits GH signaling by suppressing GH-induced JAK2 phosphorylation, an effect mediated by SOCS–2. *Proc. Natl. Acad. Sci. USA* **100**:1016–1021.

Liu C, Grossman A, Bain S, et al. (1997) Leptin stimulates cortical bone formation in obese mice. *J. Bone Miner. Res.* **12**:S83.

MacDonald SM, Reeder BA, Chen Y, and Depres JP (1997) Obesity in Canada: A descriptive Analysis. *Can. Med. Assoc. J.* **145**:S39–S45.

Manolagas SC and Jilka RL (1995) Bone marrow, cytokines, and bone remodelling. Emerging insights into the pathophysiology of osteoporosis. *N. Engl. J. Med.* **332**:305–311.

Marcus C, Margery V, Kamel A, Bronnegard M (1994) Effects of growth hormone on lipolysis in humans. *Acta. Paediatr.* **406**(Suppl): 54–58.

Marcus R (1997) Skeletal effects of growth hormone and IGF-I in adults. *Horm. Res.* **48**:60–64.

Martin RB, Chow BD, Luca PA (1990) Bone marrow fat content in relation to bone remodelling and serum chemistry in intact and ovariectomized dogs. *Calcif. Tissue Int.* **46**:189–194.

Mathey J, Horcajada-Molteni MN, Chanteranne B, Picherit C, Puel C, Lebecque P, et al (2002) Bone mass in obese diabetic Zucker rats: influence of treadmill running. *Calcif. Tissue Int.* **70**:305–311.

McCalden RW, RcGeough JA, Barker MB, and Court-Brown CM (1993) Age–related changes in the tensile properties of cortical bone. The relative importance of changes in porosity, mineralization, and microstructure. *J. Bone Joint Surg. Am.* **75**:1193–1205.

McNeillie EM and Zammit VA (1982) Regulation of acetyl–CoA carboxylase in rat mammary gland. *Biochem. J.* **204**:273–288.

Mohan S, Baylink DJ. 1999. Role of Growth Hormone/Insulin-like Growth Factor Axis. In: The Aging Skeleton. CJ Rosen, J Glowacki, JP Bilezikian, eds. Academic Press, publisher, Toronto. pp 209–219.

Moller N, Jorgensen JO, Alberti KG, Flyvbjerg A, and Schmitz O (1990) Short–term effects of growth hormone on fuel oxidation and regional substrate metabolism in normal man. *J. Clin. Endocrinol. Metab.* **70**:1179–1186.

Morel G, Chavassieux P, Barenton B, Dubois PM, Meunier PJ, and Boivin G (1993) Evidence for a direct effect of growth hormone on osteoblasts. *Cell Tissue Res.* **273**:279–286.

Morris HA, Porter SJ, Durbridge TC, Moore RJ, Need AG, and Nordin BE (1992) Effects of oophorectomy on biochemical and bone variables in the rat. *Bone Miner.* **18**:133–142.

Mosekilde L, Thomsen JS, Orhii PB, and Kalu DN (1998). Growth hormone increases vertebral and femoral bone strength in osteopenic, ovariectomized, aged rats in a dose–dependent and site–specific manner. *Bone* **23**:343–352.

Mosekilde L, Thomsen JS, Orhii PB, McCarter RJ, Mejia W, and Kalu DN (1999) Additive effect of voluntary exercise and growth hormone treatment on bone strength assessed at four different skeletal sites in an aged rat model. *Bone* **24**:71–80.

Nagy TR, Prince CW, and Li J (2001) Validation of peripheral dual–energy X–ray ab-

sorptiometry for the measurement of bone mineral in intact and excised long bones of rat. *J. Bone Miner. Res.* **16**:1682–1687.

Natera SH, Jiang WJ, Ng FM (1994) Reduction of cumulative body weight gain and adipose tissue mass in obese mice: response to chronic treatment with synthetic hGH 177–191 peptide. *Biochem. Mol. Biol. Int.* **33**:1011–1021.

Ng FM, Bornstein J, Welker C, Zimmet PZ, and Taft P (1974) Insulin potentiating action of synthetic peptides relating to the amino terminal sequence of human growth hormone. *Diabetes* **23**:943–949.

Ng FM (1990) Human growth hormone fragments. In New Antidiabetic Drugs (Bailey CJ and Flatt PR., eds). Smith-Gordon, London; Nishimura, Niigata-Shi, Japan, pp.197–209.

Ng FM, Sun J, Sharma L, Libinaka R, Jiang WJ, Gianello R (2000) Metabolic studies of a synthetic lipolytic domain (AOD9604) of human growth hormone. *Horm. Res.* **53**:274–8.

Ng FM, Jiang WJ, Gianello R, Pitt S, Roupas P (2000b) Molecular and cellular actions of a structural domain of human growth hormone (AOD9401) on lipid metabolism in Zucker fatty rats. *J. Mol. Endocr.* **25**:287–298.

Nishiyama K, Sugimoto T, Kaji H, Kanatani M, Kobayashi T, and Chihara K (1996) Stimulatory effect of growth hormone on bone resorption and osteoclast differentiation. *Endocrinology* **137**:35–41.

Nuttall ME, Gimble JM (2000) Is there a therapeutic opportunity to either prevent or treat osteopenic disorders by inhibiting marrow adipogenesis? *Bone* **27**:177–184.

Ogru E, Wilson JC, Heffernan M, Jiang WJ, Chalmers DK, Libinaki R, Ng F (2000) The conformational and biological analysis of a cyclic anti–obesity peptide from the C–terminal domain of human growth hormone. *J. Peptide Res.* **56**:388–397.

Ohlsson (2002) A Model for Tissue-Specific Inducible Insulin-like Growth Factor–I (IGF–I) Inactivation to Determine the Physiological Role of Liver–Derived IGF–I. *Endocrine* **19**:249–256.

Okazaki R, Inoue D, Shibata M, Saika M, Kido S, Ooka H, Tomiyama H, Sakamoto Y, Matsumoto T (2002) Estrogen promotes early osteoblast differentiation and inhibits adipocyte differentiation in mouse bone marrow stromal cell lines that express estrogen receptor (ER) alpha or beta. *Endocrinology* **143**:2349–2356.

Palidini AC, Pena C and Retegui LA (1979) The intriguing nature of multiple actions of growth hormone. *Trends in Biochemical Sciences* 4:256–260.

Parfitt AM (1987) Trabecular bone architecture in the pathogenesis and prevention of fracture. *Am. J. Med.* **82**:68–72.

Pouilles JM, Tremollieres F, Todorovsky N, and Ribot C (1991) Precision and sensitivity of dual–energy x–ray absorptiometry in spinal osteoporosis. *J. Bone Miner. Res.* **6**:997–1002.

Reid, I (2004) Leptin deficiency - Lessons in regional differences in the regulation of

bone mass [perspective]. *Bone* **34**:369–371.

Reseland JE, Gordeladze JO, Drevon CA. (2002) Leptin receptor (OB-R) gene expression in human primary osteoblasts: reaffirmation. *J. Bone Miner. Res.* **17**:1136.

Richelsen B (1997) Action of growth hormone in adipose tissue. *Horm. Res.* **48** (Suppl5): 105–110.

Ridderstrale M and Tornqvist H (1996) Effect of tyrosine kinase inhibitors on tyrosine phosphorylations and the insulin–like effects in response to human growth hormone in isolated rat adipocytes.*Endocrinology* **137**:4650–4656.

Roseland JE, Gordeladze JO, Drevon CA (2002) Leptin receptor (OB-R) gene expression in human primary osteoblasts: reaffirmation. *J. Bone Miner. Res.* **17**:1136.

Roupas P, Chou SY, Towns RJ and Kostyo JL (1991) Growth hormone inhibits activation of phosphatidylinositol phospholipase C in adipose plasma membranes: evidence for a growth hormone–induced change in G protein function. *PNAS* **88**:1691–1695.

Roupas P and Herington AC (1994) Postreceptor signaling mechanisms for growth hormone. *Trends in Endocrinology and Metabolism* **5**:154–158.

Rui L, Mathews LS, Hotta K, Gustafson TA and Carger-Su C (1997) Identification of SH2-β as a substrate of the tyrosine kinase JAK2 involved in growth hormone signaling. *Molecular and Cellular Biology* **17**:6633–6644.

Saika M, Inoue D, Kido S, Matsumoto T (2001) 17 beta-estradiol stimulates expres-

sion of osteoprotegerin by a mouse stromal cell line, ST-2, via estrogen receptor-alpha. *Endocrinology* **42**: 2205–2212.

Sato M, McClintock C, Kim J, Turner CH, Bryant HU, Magee D, and Slemenda CW (1994) Dual–energy x–ray absorptiometry of raloxifene effects on the lumbar vertebrae and femora of ovariectomized rats. *J. Bone Miner. Res.* **9**:715–724.

Scanes CG and Campell RM (1995) Growth Hormone: Chemistry. In:Growth Hormone. CRC Press.

Schenk RK, Olah AJ, and Herrmann W (1994) Preparation of calcified tissues for light microscopy. In: Dickson GR, ed. Methods of Calcified Tissue Preparation. New York: Elsevier. pp 1–56.

Kaplan FS, Hayes WC, Keaveny TM, Boskey A, Einhorn TA, Iannotti JP. 1994. Form and Function of Bone. In: Orthopaedic Basic Science. SR Simon, ed. American Academy of Orthopaedic Surgeions, Publisher, Columbus, Ohio. pp.127–184.

Siegrist-Kaiser CA, Pauli V, Juge-Aubry JA, Boss O et al (1997) Direct Effects of Leptin on Brown and White Adipose Tissue. *J. Clin. Invest.* **100**: 2858-2864.

Serra J (1988) Image Analysis and Mathematical Morphology, Vol. 1. Academic Press, London.

Shen V, Birchman R, Xu R, Lindsay R, and Dempster DW (1995) Short-term changes in histomorphometric and biochemical turnover markers and bone mineral density in estrogen-and/or dietary calcium-deficient rats. *Bone* **13**:149–156.

Slootweg MC, Swolin D, Netelenbos JC, Isaksson OG Ohlsson C (1997). Estrogen enhances growth hormone receptor expression and growth hormone action in rat osteosarcoma cells and human osteoblast-like cell. *J. Endorcrinol.* **155**:159–164.

Spelsberg TC, Subramaniam M, Riggs BL, Khosla S (1999) The actions and interactions of sex steroids and growth factors/cytokines on the skeleton. *Mol. Endocrinol.* **13**:819–828.

Statistics Canada (2004) Canadian Community Health Survey Cycle 2.2.

Steppan CM, Crawford DT, Chidsey-Frink KL, Ke HZ, Swick AH (2000) Leptin is a potent stimulator of bone growth in ob/ob mice. *Regul. Pept.* **92**:73–78.

Suliman IA, EI Bakri NK, Adem A, Mustafa A, Lindgren JU (2001) The effect of ovariectomy and ovarian steroid treatment on growth hormone and insulin-like growth factor-I levels in the rat femur. *J. Orthop. Res* **19**:1008–1012.

Takeda S, Elefteriour F, Levasseur R, Liu X, Zhao L, Parker KL, et al (2002) Leptin regulates bone formation via the sympathetic nervous system. *Cell* **111**:305–317.

Thomas T, Gori F, Khosla S, Jensen MD, Burguera B, Riggs BL (1999) Leptin acts on human marrow stromal cells to enhance differentiation to osteoblasts and to inhibit differentiation to adipocytes. *Enocrinology* **140**:1630–1638.

Thomsen JS, Ebbesen EN, and Mosekilde L (2002) Predicting human vertebral bone strength by vertebral static histomorphometry *Bone* **30**:502–508.

Turner CH and Burr DB. (2001) Experimental Techniques for Bone Mechanics. In: Bone Mechanics Handbook Second Edition, Cowin SC, editor. New York: CRC Press.

Turner RT, Riggs BL, and Spelsberg TC (1994) Skeletal effects of estrogen. *Endocr. Rev.* **15**:275–300.

Ultsch MH, Somers W, Kossiakoff AA and De Vos AM (1994) The Crystal Structure of Affinity–matured Human Growth Hormone at 2 Angstrom Resolution. *J. Mol. Biol.* **236**:286–299.

Verhaeghe J, van Bree R, Van Herck E, Thomas H, Skottner A, Dequeker J, Mosekilde L, Einhorn TA, and Bouilllon R (1996) Effects of recombinant human growth hormone and insulin–like growth factor–I, with or without 17 beta–estradiol, on bone and mineral homeostasis of aged ovariectomized rats. *J. Bone Miner. Res.* **11**:1723–1735.

Wahner H (1989) Technical aspects and clinical interpretation of bone mineral measurements. *Public Health Rep.* **104** Suppl:27–30.

Wang L, Orhii PB, Banu J, and Kalu DN (2001) Bone anabolic effects of separate and combined therapy with growth hormone and parathyroid hormone on femoral neck in aged ovariectomized osteopenic rats. *Mech. Aging Dev.* **122**:89–104.

Wasnich RD (1996) Epidemiology of osteoporosis. In: Favus MJ, ed. Primer on the Metabolic Bone Diseases and Disorders of Mineral Metabolism. Philadelphia: Lippincott-Raven. pp 249–251.

Weiner S, Arad T, Sabanay I, Traub W (1997) Rotated Plywood of Primary Lamellar Bone in the Rat: Orientations of the Collagen Fibril Arrays. *Bone* **20**:509–514.

Whitfield JF. (2001) Leptin: brains and bones. *Exp. Opin. Invest. Drugs* **10**:1617–1622.

Wijaya E and Ng FM (1993) Effect of an antilipogenic fragment of human growth hormone on glucose transport in rat adipocytes. *Biochem. Mol. Biol. Int.* **31**:543–52.

Wroblewski VJ, Masnyk M, and Becker GW (1991) Proteolytic cleavage of human growth hormone (hGH) by rat tissues in vitro: influence on the kinetics of exogenously administered hGH. *Endocrinology* **129**:465–474.

Wronski TJ and Yen CF (1991) The ovariectomized rat as an animal model for postmenopausal bone loss. *Cells and Materials* **Suppl1**:69–74.

Wu Z and Ng FM (1993). Antilipogenic action of synthetic C–terminal sequence 177–191 of human growth hormone. *Biochem. Mol. Biol. Int.* **30**:187–196.

Yeh JK, Chen MM, and Aloia JF (1997) Effects of estrogen and growth hormone on skeleton in the ovariectomized rat with hypophysectomy. *American Journal of Physiology* **273**: t–42.